NASA
Technical
Paper
3125

November 1991

A Comparison of Airborne Wake Vortex Detection Measurements With Values Predicted From Potential Theory

Eric C. Stewart

NASA

[redacted]

NASA Technical Paper 3125

1991

A Comparison of Airborne Wake Vortex Detection Measurements With Values Predicted From Potential Theory

Eric C. Stewart
Langley Research Center
Hampton, Virginia

NASA
National Aeronautics and Space Administration
Office of Management
Scientific and Technical Information Program

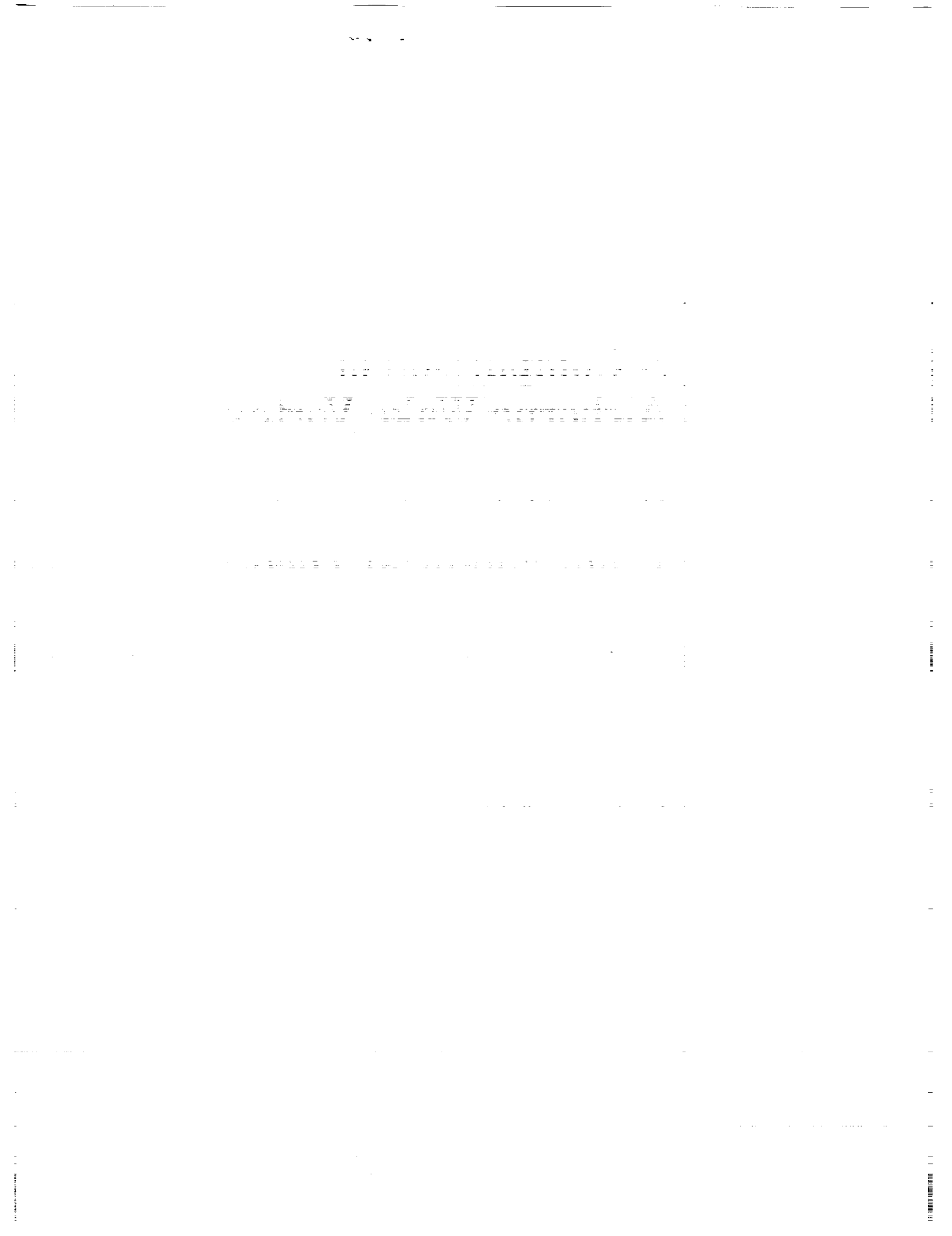

Abstract

An analysis of flight measurements made near a wake vortex was conducted to explore the feasibility of providing a pilot with useful wake-avoidance information. The measurements were made with relatively low-cost flow and motion sensors on a light airplane flying near the wake vortex of a turboprop airplane weighing approximately 90 000 lb. Algorithms were developed which removed the response of the airplane to control inputs from the total airplane response and produced parameters which were due solely to the flow field of the vortex. These parameters were compared with values predicted by potential theory. The results indicated that the presence of the vortex could be detected by a combination of parameters derived from the simple sensors. However, the location and strength of the vortex cannot be determined without additional and more accurate sensors.

Introduction

The limited rate at which airplanes can land at an airport is a serious problem facing the commercial airplane industry, particularly in Instrument Meteorological Conditions (IMC). One factor which limits the landing rate is the Instrument Flight Rules (IFR) longitudinal spacing required between trailing airplanes in the landing pattern. These longitudinal spacing requirements were imposed to reduce the operational hazard which might be associated with the vortices trailing from the wingtips. One proposed solution for this problem is to provide the pilot with warning and avoidance information should the airplane approach a dangerous vortex. A theoretical analysis indicated that, using conventional airborne sensors, a warning could be generated at a distance which would provide the pilot with ample time to avoid the vortex (ref. 1). Angle of attack and angle of sideslip sensors mounted on the detecting airplane were thought to be sufficient by themselves for measuring the vertical and horizontal components of the vortex velocity, while airplane rolling sensors could be used to measure the lateral gradient of the vertical component of the vortex velocity. These velocity components and gradients could then be used in closed-form equations based on a dipole approximation of the wake vortex to determine the location and strength of the wake vortex. Depending on the accuracy of the sensors, it was predicted that the wake vortex of a large airplane could be detected, located, and quantified at a distance of almost 500 ft.

The National Aeronautics and Space Administration (NASA) and the Federal Aviation Administration (FAA) recently undertook a flight test to investigate these concepts. The preliminary analyses of the flight data indicated that, under certain circumstances, the vortex field could be detected, although at smaller distances than had been anticipated (refs. 2 and 3). These preliminary analyses were based on postflight inspections of time histories of the flight data and did not attempt to locate or determine the strength of the wake vortices by using only the sensors on the detecting airplane. This paper presents a more detailed analysis of the same flight data. The primary purposes of the present analysis were (1) to develop candidate vortex flow parameters and algorithms and (2) to determine if the location and strength of the vortex could be determined theoretically as well as experimentally with a combination of vortex flow parameters.

Measurements on the detecting airplane of the flow angles, velocity, angular rates, attitude, and control position were used in the algorithms. These algorithms produced the following vortex flow parameters: differential angle of attack, differential angle of sideslip, angle of attack, vertical velocity, and rolling rate. A potential theory model with two vortices rotating in opposite directions was used to calculate theoretical values of the vortex flow parameters for comparison with the measured vortex parameters. In addition, the potential model was used to determine the theoretical combination of parameters required to ascertain the location and strength of the wake vortex as well as to develop an estimate of the distance at which a warning of a vortex presence could be generated.

Symbols

A_N, A_x, A_y	accelerations of detecting airplane referenced to body axes, g units
b_d	span of detecting airplane, ft
b_g	span of airplane generating wake vortex, ft
b_s	separation vortices in wake vortex pair, ft
C_{l_p}	roll damping coefficient, -0.49 per rad
d	horizontal distance from nearest vortex of vortex pair to c.g. of detecting airplane (always positive at the beginning of a run), ft
Δd	warning distance of vortex presence provided by sensors, ft (see eq. (12))

d_{k_1}, d_{k_2}	distance at which nondimensional roll rate due to vortices is equal to k_1 or k_2, ft
h	altitude of detecting airplane, ft
$\dot{h}_m$	measured vertical velocity (determined by differentiating pressure altitude)
$\dot{h}_{\text{still air}}$	vertical velocity in still air, ft/sec
$\dot{h}_v$	vertical velocity due to vortex pair, ft/sec
I_x	roll moment of inertia, slug-ft^2
k	detection threshold value
k_1, k_2	fractions of lateral control parameter (see eq. (12))
L_g	lift on generating airplane, lbf
p, q, r	rolling, pitching, and yawing rates of detecting airplane (positive to right, up, and right, respectively), rad/sec or deg/sec
p_v	rolling rate due to vortices (positive right wing down), rad/sec or deg/sec
p_{δ_a}	rolling rate due to aileron input (positive right wing down), rad/sec
R	radial distance from center of vortex dipole to c.g. of detecting airplane, ft
r	radial distance from center of a single vortex, ft
$r_{i,j}$	radial distance from vortex j to location i on detecting airplane, ft
S_d	wing area of detecting airplane, ft^2
s	Laplace variable, sec^{-1}
u, v, w	longitudinal, lateral, and vertical velocity components in body axis system of detecting airplane, ft/sec (see appendix)
V	true airspeed, ft/sec
V_d	true airspeed of detecting airplane, ft/sec
V_g	true airspeed of wake vortex generating airplane, ft/sec
V_θ	tangential velocity component due to a single vortex (always positive), ft/sec
$V_{\theta_{i,j}}$	tangential velocity at ith location on detecting airplane due to jth vortex, ft/sec
v	lateral velocity due to wake vortex in X, Y, Z Earth-fixed axis system, ft/sec
$v_{\theta_{i,j}}$	lateral velocity in detecting airplane reference system at ith wingtip due to jth vortex, ft/sec
W_g	weight of wake vortex-generating airplane, lb
w	vertical velocity due to wake vortex in X, Y, Z Earth-fixed axis system, ft/sec
$w_{\theta_{i,j}}$	vertical velocity in detecting airplane reference system at ith wingtip due to jth vortex
X, Y, Z	Earth-fixed axis system (figs. 1 and 5)
y, z	coordinates of detecting airplane in Earth-fixed axis system, ft (figs. 1 and 5)
α	angle of attack, rad
$\Delta\alpha$	difference between vortex-induced angle of attack at right wingtip and vortex-induced angle of attack at left wingtip, rad or deg
$\alpha_{\theta_{i,j}}$	angle of attack at ith wingtip due to jth vortex, rad
α_v	angle of attack due to vortex as determined from wingtip flow sensors, rad or deg
$\alpha_{\delta_{\text{stab}}}$	angle of attack due to stabilator inputs, rad
β	angle of sideslip
$\beta_{\theta_{i,j}}$	angle of sideslip at ith wingtip due to jth vortex, rad
$\Delta\beta$	difference between vortex-induced angle of sideslip at right wingtip and vortex-induced angle of sideslip at left wingtip, rad or deg
Γ	circulation of wake vortex, ft^2/sec
δ_a	aileron position (positive trailing edge down on right wing), deg

δ_{stab}	stabilator position (positive trailing edge down), deg
δ_r	rudder position (positive trailing edge to left), deg
ζ	angular position of c.g. of detecting airplane with respect to center of vortex pair, deg
θ	pitch attitude (positive nose up), deg (see fig. 14(c))
$\theta_{i,j}$	angle between $r_{i,j}$ and the line passing through the centers of the vortices, rad (see fig. 5)
ρ	density of air, slug/ft^3
ρ_o	sea level standard density of air, 0.002378 slug/ft^3
σ	relative air density, ρ/ρ_o
τ	rolling mode time constant, sec
ϕ	roll attitude of detecting airplane (positive right wing down), rad

Subscripts:

C	corrected
c.g.	center of gravity
d	detecting airplane
g	vortex-generating airplane
i	index indicating location on detecting airplane, 1 = right wingtip, 2 = left wingtip, 3 = c.g.
j	index indicating vortex, 1 = right vortex, 2 = left vortex, as viewed from rear
L	left wingtip of detecting airplane
lag	first-order lag
M	measured
R	right wingtip of detecting airplane
v	due to vortex
θ	due to tangential velocity of flow around a single vortex

Abbreviations:

FDV	flow direction and velocity
IMC	Instrument Meteorological Conditions
IFR	Instrument Flight Rules

Flight Tests and Data Processing

Flight Tests

The flight test arrangement and axis system used in the present study are shown in figure 1. A more complete description of the flight tests is given in reference 3. All tests were conducted at NASA's Wallops Flight Facility. Three airplanes were used. The vortex-generating airplane was a Lockheed P-3 (fig. 2) fitted with smoke-generating apparatus on each wingtip. The P-3 weighed about 91 500 lb in the test configuration and had a wingspan of 99.8 ft. The detecting airplane was a Piper PA-28 which weighed about 2400 lb and had a wingspan of 35.43 ft (fig. 3). The PA-28 had been used previously in NASA's general aviation stall/spin program (ref. 4). In the present study, the research instrumentation described in reference 4 was used with minimal modification. For example, the only modification to the flow direction and velocity (FDV) sensors mounted on the wingtip booms was to scale them for smaller angles of attack. A list of the measurements made on the PA-28 is presented in table I. It should be noted that the resolution of the measurements shown in table I was limited by the onboard digitizing process. That is, regardless of the resolution of the individual sensors, the maximum resolution was limited to 1/256 of full scale. The third airplane, a Beechcraft T-34C (see fig. 4), was used to photograph the position of the PA-28 detecting airplane relative to the smoke entrained in a single vortex from the P-3. The T-34C was fitted with down-looking cameras on each wingtip that recorded video images from which the relative horizontal distances between vortex and detecting airplane could be determined (ref. 5).

Before the P-3 was launched for a data-taking flight, one of the other airplanes was flown at the test altitude to determine if there was significant turbulence. If the pilot judged the turbulence to be minimal, a data-taking operation was begun. The P-3 and the PA-28 were flown at approximately the same speed (110–130 knots) and altitude (5000 ft) with the PA-28 positioned about 1.5 miles behind the P-3. The smoke generators on the P-3 were turned on individually to maximize the data-collecting time on each flight. With the previously mentioned precautions to ensure the tests were conducted in minimal turbulence, the smoke trails in the vortices appeared to have only small undulations. When the smoke generator on the right wing of the P-3 was used as shown in figure 1, the PA-28 was initially positioned about 500 ft to the right of the P-3. The PA-28 then made shallow approaches moving laterally to the left. When the smoke generator

on the left wing of the P-3 was used, the PA-28 made approaches from the left side. The pilot attempted to maintain the same altitude as the smoke trail ($z = 0$ in fig. 1) while he closed laterally on it. The pilot attempted to maintain a lateral closure rate of about 20 ft/sec by executing a 6° heading change toward the vortex smoke trail. However, it was difficult to accurately maintain such a heading, with the result the closure rate was sometimes over 40 ft/sec. Because of the disturbing influence of the wake of the P-3 on the PA-28 and/or the slight undulations of the wake itself, the pilot could not exactly maintain the correct relative altitude. A measurement of this difference in altitude could not be obtained from the photographic data taken from the T-34C, which was flying about 500 ft above the PA-28. The vertical position has a strong effect on the detection parameters, as will be shown later. Flight tests were conducted for both the "flaps retracted" and "flaps extended" configurations of the P-3 airplane.

The data from the PA-28 onboard instrumentation were merged after the flight with the lateral separation distances obtained from the T-34C camera data to produce time histories for further analysis.

Flight Data Processing

The equations used in reducing the data measured on the PA-28 are given in the appendix. The equations used for correcting the raw measurements for the influence of the flow field and the rotational motions of the detecting airplane (sections I and II) are taken from reference 6. After these conventional corrections were made, the five vortex detection parameters were calculated as shown in sections III through VI. For example, the flow angles were calculated directly from the corrected velocity components at each wingtip. The difference between the two wingtip flow angles is due to the velocity gradients in the vortex flow field. These differences, called the "differential angle of attack" ($\Delta\alpha$) and the "differential sideslip" ($\Delta\beta$), are the first two vortex detection parameters. The vortex detection parameters for angle of attack, roll rate, and vertical speed were calculated in a slightly different manner. For example, the angle of attack was calculated in two steps. First, a theoretical angle of attack $\alpha_{\delta_{\text{stab}}}$ due to longitudinal maneuvering of the airplane was calculated. For the fixed configurations and airspeed used in these test runs, a simple linear relationship between the stabilator position and the angle of attack was assumed to exist. The constants in the linear relationship were determined during early portions of selected data runs in which the detecting airplane was at a great distance from the vortex. The angle of attack due to the vortex was then taken to be equal to the measured angle of attack minus this theoretical angle of attack. A similar procedure was used for the roll rate parameter p_v except the theoretical roll rate p_{δ_a} included a correction for the transient response to an aileron input. The transient response was approximated by a first-order lag digital filter. Finally, the vertical velocity in still air was calculated from the airspeed, flow angles, and airplane attitude. The vertical velocity vortex parameter $\dot{h}_v$ was equal to the measured vertical velocity minus the vertical velocity in still air. The measured vertical velocity was taken to be the differentiated altitude derived from the static pressure sensor on the detecting airplane.

Theory

Potential theory was used to predict values of the vortex detection parameters. The entire circulation generated by the lift was assumed to be contained, without losses, in two vortices of opposite signs trailing from the tips of the wing. The geometry assumed in this analysis is presented in figure 5, which shows the view from the rear. The wake was assumed to consist of a pair of vortices which were parallel and contained in a horizontal plane. The longitudinal axis of the detecting airplane was assumed to be parallel to the vortex pair. The centers of the vortices were on a horizontal line separated by a distance of $b_s = \frac{\pi}{4} b_g$, a result of assuming an elliptic lift distribution. The magnitude of the circulation of each vortex is approximately

$$|\Gamma| = \frac{4}{\pi} \frac{L_g}{\rho V_g b_g} \tag{1}$$

where in the steady state the lift equals the weight, $L_g = W_g$.

The tangential velocity component V_θ due to each vortex is given by

$$V_\theta = \frac{|\Gamma|}{2\pi r} \tag{2}$$

where r is the radius from a vortex center to the position the tangential velocity is calculated. Tangential velocity was calculated for the four possible combinations of the two wingtips and the two trailing vortices. The generalized equation for these velocities was derived from equation (2) by accounting for the opposite directions of rotation of the two vortices to produce

$$V_{\theta_{i,j}} = (-1)^{j+1} \left(\frac{1}{2\pi r_{i,j}} \right) |\Gamma| \tag{3}$$

where $r_{i,j}$ is the radius from each vortex center to the detecting airplane (i = 1, 2, 3 indicates the right wingtip, left wingtip, and center of gravity of the detecting airplane, respectively; j =1, 2 indicates the right and left vortices, respectively). Each tangential velocity was resolved into a vertical component $w_{\theta_{i,j}}$ in the airplane axis system and converted to angle of attack as shown below:

$$\alpha_{\theta_{i,j}} = \frac{w_{\theta_{i,j}}}{V_d} = \frac{V_{\theta_{i,j}} \cos\left(\theta_{i,j} - \phi\right)}{V_d} \tag{4}$$

where $\theta_{i,j}$ and ϕ are shown in figure 5. A similar calculation can be made for the angle of sideslip:

$$\beta_{\theta_{i,j}} = \frac{v_{\theta_{i,j}}}{V_d} = \frac{-V_{\theta_{i,j}} \sin\left(\theta_{i,j} - \phi\right)}{V_d} \tag{5}$$

Using equation (4), the angle of attack due to the vortex α_v, can be approximated by

$$\alpha_v = \frac{1}{2}\left(\alpha_R + \alpha_L\right)$$

or

$$\alpha_v = \frac{1}{2}\left[\left(\alpha_{\theta_{1,1}} + \alpha_{\theta_{1,2}}\right) + \left(\alpha_{\theta_{2,1}} + \alpha_{\theta_{2,2}}\right)\right] \tag{6}$$

The vertical and lateral components of the wake vortex velocity in the Earth-fixed axis system are given by

$$w = -\left(V_{\theta_{3,1}} \cos\ \theta_{3,1} + V_{\theta_{3,2}} \cos\ \theta_{3,2}\right) \tag{7a}$$

and

$$v = \left(V_{\theta_{3,1}} \sin\ \theta_{3,1} + V_{\theta_{3,2}} \sin\ \theta_{3,2}\right) \tag{7b}$$

It should be noted that the measured vertical vortex velocity $\dot{h}_v$ discussed earlier is theoretically equal to the negative of w; i.e., $\dot{h}_v = -w$. Using equation (4), the difference in the angle of attack between the right and left wingtips of the detecting airplane can be determined:

$$\Delta\alpha = \alpha_R - \alpha_L$$

or

$$\Delta\alpha = \left[\left(\alpha_{\theta_{1,1}} + \alpha_{\theta_{1,2}}\right) - \left(\alpha_{\theta_{2,1}} + \alpha_{\theta_{2,2}}\right)\right] \tag{8}$$

Likewise, equation (5) can be used to determine the difference in the angle of sideslip between the right and left wingtips:

$$\Delta\beta = \beta_R - \beta_L$$

or

$$\Delta\beta = \left[\left(\beta_{\theta_{1,1}} + \beta_{\theta_{1,2}}\right) - \left(\beta_{\theta_{2,1}} + \beta_{\theta_{2,2}}\right)\right] \tag{9}$$

The difference in the angle of attack (eq. (8)) is approximately equal to the incremental velocity generated by a rolling rate divided by the velocity:

$$\Delta\alpha \approx \frac{pb_d}{V_d} \tag{10}$$

Thus, a theoretical rolling rate due to the presence of the vortex pair, p_v, is given by

$$p_v = -\left(\frac{V_d}{b_d}\right)\Delta\alpha \tag{11}$$

where the negative sign is introduced to account for the fact that the detecting airplane will roll in the direction that reduces the differential angle of attack. The rolling rate and the differential angle of attack can be used interchangeably to detect the presence of a vortex because they are directly related to each other. However, the rolling rate would usually be easier to measure. Measuring both the differential angle of attack and the rolling rate could provide redundant or backup information.

It should be noted that there is no equivalent relationship between the yaw rate and the differential sideslip angle or between the pitch rate and differential sideslip angle. There is no such relationship because the yaw and pitch rates do not induce differential sideslip angles at the wingtips.

These equations can also be used to develop an alternate estimate of the maximum amount of warning that could be provided to a pilot using these measurements. Rather than basing these estimates on the accuracy of the sensors making the measurements as was done in reference 1, the following analysis uses fractions of the nondimensional lateral control effectiveness parameter $\frac{pb_d}{2V_d}$ as the criteria. This parameter represents the maximum nondimensional roll rate the pilot can command and has a value of 0.06 to 0.07 for all cargo-type airplanes (ref. 7). The warning distance Δd will be defined as the difference between the distance at which the vortex is first detected and the distance at which an arbitrary fraction of the pilot's roll control authority can be overpowered by the vortex. As stated above, the first detection distance d_{k_1} can be logically defined as a fraction k_1 of the lateral control parameter. Likewise, the distance d_{k_2} at which an arbitrary fraction of the pilot's roll control authority can be overpowered can be defined as

k_2 times the maximum lateral control parameter:

$$\Delta d = d_{k_1} - d_{k_2} \tag{12}$$

In the case where the wake vortex is not strong enough to overpower the roll control authority of the detecting airplane, d_{k_2} will be assumed to be zero.

Results

Theoretical Predictions

Theoretical calculations of the vortex detection parameters were made to determine fundamental relationships and guide the interpretation of the flight test results presented later. The calculations were made for conditions which closely correspond to the actual flight test conditions with the P-3 airplane as the vortex-generating airplane and the PA-28 as the vortex-detecting airplane:

$W_g = 95\,500$ lb	$b_d = 35.43$ ft
$b_g = 99.8$ ft	$V_d = 218$ ft/sec
$V_g = 236$ ft/sec	$\sigma = 0.861$

The theoretical flow angles for the ideal situation ($z = 0$ and $\phi = 0$, fig. 5) are shown in figure 6. At distances over 200 ft, the magnitude of the angle of attack α_v is much larger than that of the differential angle of attack $\Delta\alpha$. It can be shown that at distances over about two times the vortex pair separation distance, the angle of attack α_v varies approximately as the inverse square of the distance to the center of the vortex pair. The differential angle of attack $\Delta\alpha$ varies approximately as the inverse cube of the distance. As long as the airplane is at the same altitude as the vortex pair, the differential sideslip angle $\Delta\beta$ is zero.

The effect of moving tangentially at a constant radial distance from the center of the vortex pair is shown in figure 7. The frequency of variation of the differential flow angles is about 1.5 times that of the angle of attack. It should be noted that for positions where $\Delta\alpha$ is small $\Delta\beta$ is large, and vice versa. Thus, as the differential angle of attack becomes less sensitive to the presence of the vortex pair, the angle of sideslip becomes more sensitive to the vortex pair. In other words, both $\Delta\alpha$ and $\Delta\beta$ are necessary to detect the presence of the vortex for all locations.

The effect of the roll attitude on the flow angles is presented in figure 8. As the differential angle of attack becomes smaller or less sensitive, the differential angle of sideslip becomes larger or more sensitive. The important fact is that the roll attitude has a significant effect on both angles. This means that if roll maneuvering is present, the roll attitude must be known in order to properly interpret the differential flow angles. It also has a significant implication on the controls-free response of an airplane approaching a vortex. Since the rolling moment on the approaching airplane is proportional to $\Delta\alpha$, the rolling moment will be a function of the roll attitude. Therefore, if the controls are held fixed, the airplane will roll to an attitude where $\Delta\alpha$ is zero.

Contours of constant differential flow angles with the wings level ($\phi = 0$) on the detecting airplane are shown in figure 9. The differential flow angles increase very rapidly as the vortex core is approached. The contours of each differential flow angle merge along lines labeled $\Delta\alpha = 0$ or $\Delta\beta = 0$, where the flow angles change sign. As an airplane crosses one of the $\Delta\alpha = 0$ lines near the vortices, it will experience large rolling moments which change direction rapidly.

Contours of differential flow angles of $\pm 0.1°$ are presented in figure 10. Each differential flow angle ($\Delta\alpha$ or $\Delta\beta$) has lobes of alternating sign spaced approximately every 60° around the center of the vortex pair. Each lobe of the differential angle of sideslip $\Delta\beta$ is offset about 30° from the adjacent lobe for differential angle of attack $\Delta\alpha$. This pattern produces 12 sectors based on the flow angle signs, as shown in figure 11. Therefore, the signs of the flow angles do not uniquely define the position of the vortex relative to the detecting airplane. In fact, any one combination of differential flow angles could theoretically indicate any one of three possible relative locations. Obviously, more information is needed to determine the location of the vortex pair.

Another aspect of figure 11 is that there are six approach paths along which the differential angle of attack is zero. Since the differential angle of attack is what causes most of the rolling response of the detecting airplane there would be virtually no rolling response along these loci. Although the differential angle of sideslip would be large along these loci, differential sideslip does not produce large rolling moments. Therefore, there would be no rolling motion which could warn the pilot that he was approaching a vortex.

Measurements of vertical and horizontal velocity components (w, v) can provide the additional information needed to locate the vortex pair, as shown in figure 12. By considering the signs of the four

parameters ($\Delta\alpha$, $\Delta\beta$, w, and v), the location (y, z), as well as the strength Γ and the vortex separation distance b_s, can be uniquely determined. An ideal wake vortex detection system could determine all four of these parameters. However, fewer parameters may be useful in some cases. For example, if the pilot suspected from visual or other means that a dangerous wake vortex was possibly below him during a final approach, knowing from ($\Delta\alpha$ and $\Delta\beta$) that he was indeed approaching a vortex pair could be useful.

Formulas for determining the location (y, z) in terms of only three measurements (w, v, and $\frac{dw}{dy}$ or $\Delta\alpha$) are given in reference 1. Three rather than four measurements were sufficient in these formulas because a dipole approximation (in which Γ and b_s were combined into their product) was used in the development of the formulas. Although these formulas are theoretically correct, they are impractical for measurements with any uncertainty because they contain divisions by numbers which can be theoretically (as well as practically very nearly) equal to zero. With any uncertainty in the measurements, three measurements will produce two possible locations.

The maximum theoretical warning distance provided by the rolling rate (or differential angle of attack) is shown in figure 13 as a function of the weight of the vortex-generating airplane. As indicated on the second abscissa of the figure, the span of the generating airplane was assumed to vary linearly with the landing weight. The constants in the linear relationship were determined using published values of weights and spans for contemporary airliners. Increasing the weight of the generating airplane, increasing the assumed sensitivity (reducing the theoretical threshold k_1), or increasing the span of the detecting airplane increases the amount of the warning. For a detecting airplane with a wingspan of 100 ft ($b_d = 100$) and the lowest threshold ($k_1 = 0.025$), the warning is approximately 200 ft for a heavy vortex-generating airplane ($W_g = 600\,000$ lb). This warning would provide about 10 sec for the pilot to take corrective action assuming a 20-fps closing rate between the detecting airplane and the vortex pair. These predictions are based on differential angle of attack measured in the horizontal plane containing the centers of the vortices. These results can be generalized to all positions if it is assumed that differential sideslip is also measured and has the same sensitivity as angle of attack. This maximum warning of 200 ft is much less than the 500 ft predicted in reference 1. Using the nondimensional roll rate parameter rather than sensor sensitivity to estimate the maximum warning seems logical because measurement contamination due to pilot inputs and random turbulence can be expressed as a fraction of the parameter. Increasing the sensitivity of the sensors will not reduce the level of this contamination or necessarily increase the detection distance.

Flight Measurements

An example of the measured flight data is presented in figure 14. As the vortex was approached (d decreasing) there was increased activity in most of the measured airplane responses. However, the pilot's control activity also increased as he attempted to maneuver the airplane in the desired fashion. Thus, the response of the airplane to the vortex was very difficult to separate from the response of the airplane to the pilot's control inputs.

Time histories of the processed detection parameters for the same data run are presented in figure 15. The differential angle of attack $\Delta\alpha$ and the rolling rate due to the vortex p_v show an apparent correlation with the horizontal displacement d. The differential sideslip $\Delta\beta$ shows very little correlation with d, possibly because the pilot may have been able to maintain the airplane close to the same altitude as the vortex. The altitude rate parameter $\dot{h}_v$ was not correlated with d for the entire run. The scale for $\dot{h}_v$ was shifted to make its average value zero in order to correct for slight biases in the measured parameters, especially the measured angle of attack and pitch attitude (see fig. 14). One possible explanation for the lack of correlation for $\dot{h}_v$ is that the altitude (and thus $\dot{h}_m$) was derived from a static pressure measurement with very low resolution (about 39 ft). The static pressure may also be modified by the presence of the vortex pair and therefore be inaccurate close to the vortex.

A cross plot of α_v in figure 15 against the horizontal distance to the vortex is presented in the "flaps retracted" part of figure 16. A similar plot for a "flaps extended" run is provided for comparison. (The flap configurations refer to the vortex-generating airplane.) The angle of attack due to the vortex is essentially zero regardless of the horizontal position and does not agree at all with the value predicted by equation (6). The cause of this disagreement is the static longitudinal stability of the detecting airplane. Although the detecting airplane is probably encountering an upward flow or increased angle of attack due to the wake vortex, the airplane pitches down into the flow. The detecting airplane will maintain its original trim angle of attack as long as the flow does not change faster than the airplane can pitch into the flow. The rate at which the airplane

can pitch into the flow is determined by the short period response of the airplane. Angle-of-sideslip vanes cannot be used to measure the horizontal vortex velocity. The directional stability of the airplane will cause the airplane to yaw into the horizontal flow and maintain its original trim angle of sideslip.

It follows that angle-of-attack and angle-of-sideslip vanes cannot by themselves measure the velocity components of the vortex flow as suggested in reference 1. Flow vanes (with airspeed) measure only the components of the local flow relative to the airplane. The components of the airplane velocity relative to an axis system moving with the wind must be known in order to determine the vortex flow velocity components. If the wind is steady, this wind-fixed axis system is practically equivalent to an Earth-fixed system. Attempts were made to determine the vertical velocity of the detecting airplane relative to an Earth-fixed system (1) by integrating the vertical accelerometer and (2) by the previously mentioned differentiation of the static pressure altitude measurement. Both attempts failed to produce usable results, probably because of the poor resolution of the instrument system used in these tests compared with the signal (vortex velocities). For long-distance, real-time vortex detection, measurements of at least the quality associated with an inertial navigation system may be required. However, it is beyond the scope of this paper to determine exactly what accuracy is required. It can only be said that the present data system was not accurate enough to allow a determination of the vortex velocity components.

A cross plot of the differential angle of attack shown in figure 14 against the horizontal distance to the vortex is presented in the "flaps retracted" part of figure 17. A similar plot for a "flaps extended" run is provided for comparison. (The flap configurations refer to the vortex-generating airplane.) Included on each plot are values calculated using equation (8) assuming the detecting airplane is in the plane of the vortex pair ($\zeta = 0$) and has a zero-roll attitude ($\phi = 0$). The agreement between the theory and the measured data is good for the flaps-retracted configuration, but for the flaps extended configuration the measured values are generally less than those predicted theoretically.

Corresponding plots for the roll rate due to the vortex p_v are presented in figure 18. The same observations can be made for p_v as were made for the differential angle of attack. In fact, p_v and $\Delta\alpha$ appear to be interchangeable as far as information is concerned. However, p_v is easier to obtain operationally, being derived from four measurements (p, δ_a, V, and σ), while nine measurements ($V_{R,M}$, α_R, $\beta_{R,M}$, $V_{L,M}$, $\alpha_{L,M}$, $\beta_{L,M}$, p, q, and r) were required for $\Delta\alpha$. The calculation for $\Delta\alpha$ could possibly be simplified by neglecting some of the smaller terms, but determining the allowable simplification was not part of this study.

Also drawn in figure 18 are horizontal lines for a detection threshold value of $k_1 = 0.05$ in equation (12). For the smooth air conditions and the gentle maneuvering in the present tests, a value of 0.05 would seem to be large enough to prevent many false alarms. Tests in turbulent conditions are needed to determine if k_1 can be lowered below a value of 0.05.

Time histories of the detection parameters for a test run which illustrates some of the concepts shown in the "Theoretical Predictions" section are presented in figure 19. In this run the pilot stated that he noticed his altitude was less than that of the smoke trail as he began his approach. He, therefore, made an "up" stabilator input to correct this error. The input was slightly larger than needed, and he soon was too high. In the meantime he was closing much more rapidly than usual on the vortex, and he actually passed over the top of the smoke trail. Thus, the horizontal displacement in figure 19 became negative before the airplane moved away from the vortex again. Unlike most of the runs, the detecting airplane traversed more than 1 or 2 of the 12 sectors shown in figure 11. Therefore, the differential flow angles and the rolling rate due to the vortex switched sign more than once in figure 19.

Cross plots of the two differential flow angles against the horizontal displacement are shown in figure 20. The differential angle of attack remained very small until the horizontal displacement was only 35 ft. It appears that the differential angle of attack confirms the pilot's report that the detecting airplane was not approaching the vortex at the same altitude as that of the vortex.

The differential angle of sideslip, on the other hand, began to indicate the presence of the vortex at about 80 ft. Thus, as the theory predicted, the differential sideslip can be used to complement the differential angle of attack when z is not zero. As the detecting airplane passed over the vortex, both angles became very large (note that the scale of fig. 20 is much larger than that of fig. 17).

The trajectory of the detecting airplane relative to the vortex pair was reconstructed using the two differential flow angles and additional information obtained from the video data. The video indicated that the detecting airplane moved from right to left as it approached the vortex from the right side of the P-3. It also showed that the PA-28 clearly passed

over the top of the vortex, even though the relative vertical distance could not be ascertained. Using this video information and the cross plot in figure 21, a trajectory was reconstructed manually by guessing coordinates for the detecting airplane relative to the vortex dipole. The trajectory developed is shown in figure 22, which shows the detecting airplane passing from the first quadrant into the second quadrant and then back to the first quadrant. The theoretical cross plot of the differential flow angles for this trajectory is shown in figure 23. The theoretical pattern in figure 23 is very similar to the measured pattern in figure 21, indicating the trajectory in figure 22 is very likely the correct one. However, if the video data had not been available, there are two other entirely different trajectories which could have exactly the same cross plot shown in figure 23. These trajectories are shown in figure 22 and are completely different from the correct one. As shown earlier, measurements of the vertical and horizontal vortex velocities, in addition to $\Delta\alpha$ and $\Delta\beta$, are necessary to uniquely define the position relative to the vortex pair. With all four of these measurements ($\Delta\alpha$, $\Delta\beta$, w, and v), the vortex strength and separation can also be determined.

Conclusions

An analysis of flight measurements of a wake vortex was conducted to explore the feasibility of providing a pilot with useful information for avoiding a wake vortex. Methods were developed to convert measurements from simple sensors into parameters due entirely to the presence of the wake vortex. These parameters were compared with values predicted from simple theory. The following conclusions were made:

1. A combination of differential angle of attack and differential angle of sideslip between the wingtips can be used to detect the presence, but not the location, of a vortex pair. Additional measurements of the vertical and horizontal velocity components of the flow field are necessary to determine a unique location of the vortex relative to the detecting airplane and to determine the strength and separation of the vortex pair. Angle of attack and angle of sideslip cannot be used by themselves to determine these vertical and horizontal velocity components of the vortex field. Measurements of the airplane velocity relative to an Earth-fixed system are also needed. The Earth-fixed airplane velocities could not be measured with sufficient accuracy using the present data system.

2. The roll rate due to the vortex is directly proportional to the differential angle of attack and can be used interchangeably with it. No analogous angular rate exists for the differential angle of sideslip.

3. Values predicted by potential theory agreed with measured differential angle of attack and roll rate for many cases in which vortices were generated with the flaps retracted. However, the agreement was not good when the flaps were extended, a case that is operationally more important.

4. Assuming a detection threshold value of 0.025, the maximum amount of theoretical warning before roll control is lost can be up to 200 ft of lateral displacement. The actual value depends on the sizes of the airplanes involved as well as the threshold values.

NASA Langley Research Center
Hampton, VA 23665-5225
August 20, 1991

Appendix

Flight Data Reduction Equations

I. Correction of flow direction and velocity (FDV) measurements:

The angles of attack were corrected for the influence of the wing on the local flow.

$$\alpha_R = 0.84\alpha_{R,M}$$

$$\alpha_L = 0.84\alpha_{L,M}$$

However, no corrections were made to the angle of sideslip or true airspeed measurements.

II. Calculate body axis velocity components and correction for rotational rates:

$$u_R = V_R \cos\beta_R \cos\alpha_R + 0.66q + 17.68r$$

$$v_R = V_R \sin\beta_R - 0.66p - 4.57r$$

$$w_R = V_R \cos\beta_R \sin\alpha_R - 17.68p + 4.57q$$

$$u_L = V_L \cos\beta_L \cos\alpha_L + 0.66q - 17.68r$$

$$v_L = V_L \sin\beta_L - 0.66p - 4.57r$$

$$w_L = V_L \cos\beta_L \sin\alpha_L + 17.68p + 4.57q$$

where the constants are the positions in feet of the FDV sensors from the center of gravity, and p, q, and r are the angular rates in rad/sec.

Calculate velocity and angle of attack of detecting airplane:

$$V_{R,C} = \sqrt{u_R^2 + v_R^2 + w_R^2}$$

$$V_{L,C} = \sqrt{u_L^2 + v_L^2 + w_L^2}$$

$$V = \left(V_{R,C} + V_{L,C}\right)/2$$

$$\alpha = \tan^{-1}\left(\frac{w_{\text{c.g.}}}{u_{\text{c.g.}}}\right)$$

$$= \tan^{-1}\left[\frac{1/2\left(w_R + w_L\right)}{1/2\left(u_R + u_L\right)}\right]$$

$$= \tan^{-1}\left(\frac{w_R + w_L}{u_R + u_L}\right)$$

III. Calculate differential flow angles due to the vortices:

$$\Delta\alpha = \tan^{-1}\left(\frac{w_R}{u_R}\right) - \tan^{-1}\left(\frac{w_L}{u_L}\right)$$

$$\Delta\beta = \sin^{-1}\left(\frac{v_R}{V_R}\right) - \sin^{-1}\left(\frac{v_L}{V_L}\right)$$

IV. Calculate angle of attack due to the vortices:

A. Calculate angle of attack due to stabilator inputs:

$$\alpha_{\delta_{\text{stab}}} = -1.85\delta_{\text{stab}} + 1.92$$

where the constants are empirically determined for the flight condition of interest away from the influence of the vortices.

B. Calculate angle of attack due to the vortices:

$$\alpha_v = \alpha - \alpha_{\delta_{\text{stab}}}$$

V. Calculate roll rate due to the vortices:

A. Calculate roll mode time constant:

$$\tau = \frac{2V_d I_x}{\left(\frac{1}{2}\sigma\rho_o V_d^2\right) S_d b_d^2} C_{l_p}$$

B. Calculate a "lagged" aileron input to account for roll dynamics:

$$(\delta_a)_{\text{lag}} = \delta_a\left(\frac{1}{1+\tau s}\right)$$

C. Calculate normal roll rate response independent of the influence of the vortices:

$$p_{\delta_a} = -\frac{V}{48}(\delta_a)_{\text{lag}}$$

where 48 is an empirically determined constant for the flight condition of interest away from the influence of the vortices.

D. Calculate the roll rate due to the vortices:

$$p_v = p - p\delta_a$$

VI. Calculate vertical velocity due to the vortices:

A. Calculate vertical velocity in still air:

$$\dot{h}_{\text{still air}} = V(\cos\beta\cos\alpha\sin\theta - \sin\beta\sin\phi\cos\theta - \cos\beta\sin\alpha\cos\phi\cos\theta)$$

B. Calculate vertical velocity due to the vortices:

$$\dot{h}_v = \dot{h}_m - \dot{h}_{\text{still air}}$$

where $\dot{h}_m$ is determined by differentiating the altitude as determined from the static pressure sensor.

Note: All the vortex detection parameters were filtered through a digital first-order lag filter to reduce noise.

References

1. Bilanin, Alan J.; Teske, Milton E.; and Curtiss, Howard C., Jr.: *Feasibility of an Onboard Wake Vortex Avoidance System.* NASA CR-187521, 1987.

2. Verstynen, Harry A.; and Patterson, James C., Jr.: Preliminary Flight Test Investigation of an Airborne Wake Vortex Detection Concept. *Technical Papers—5th AIAA/SFTE/DGLR/SETP Biannual Flight Test Conference*, May 1990, pp. 180 186. (Available as AIAA-90-1282.)

3. Branstetter, J. R.; Hastings, E. C.; and Patterson, J. C., Jr.: *Flight Test To Determine Feasibility of a Proposed Airborne Wake Vortex Detection Concept.* NASA TM-102672, FAA Rep. No. DOT/FAA/CT-TN 90/25, 1991.

4. Stough, H. Paul, III; DiCarlo, Daniel J.; and Patton, James M., Jr.: *Flight Investigation of the Effects of an Outboard Wing-Leading-Edge Modification on Stall/Spin Characteristics of a Low-Wing, Single-Engine, T-Tail Light Airplane.* NASA TP-2691, 1987.

5. Childers, Brooks A.; and Snow, Walter L.: *Video Photographic Considerations for Measuring the Proximity of a Probe Aircraft With a Smoke Seeded Trailing Vortex.* NASA TM-102691, 1990.

6. Gainer, Thomas G.; and Hoffman, Sherwood: *Summary of Transformation Equations and Equations of Motion Used in Free-Flight and Wind-Tunnel Data Reduction and Analysis.* NASA SP-3070, 1972.

7. Perkins, Courtland D.; and Hage, Robert E.: *Airplane Performance Stability and Control.* John Wiley & Sons, Inc., c.1949.

Table 1. Detecting Airplane Instrumentation System

Measurement	Type sensor	Resolution
Stabilator position, δ_{stab}, deg	Control position transducer	0.1
Aileron position, δ_a, deg	Control position transducer	0.2
Rudder position, δ_r, deg	Control position transducer	0.2
Longitudinal acceleration, A_x, g units	Accelerometer	0.004
Lateral acceleration, A_y, g units	Accelerometer	0.008
Normal acceleration, A_N, g units	Accelerometer	0.015
Right wingtip angle of attack, $\alpha_{R,M}$, deg	Flow direction vane	0.12
Left wingtip angle of attack, $\alpha_{L,M}$, deg	Flow direction vane	0.12
Right wingtip angle of sideslip, $\beta_{R,M}$, deg	Flow direction vane	0.12
Left wingtip angle of sideslip, $\beta_{L,M}$, deg	Flow direction vane	0.12
Pitch attitude, θ, deg	Gyro	0.24
Roll attitude, ϕ, deg	Gyro	0.5
Pitch rate, q, deg/sec	Rate gyro	0.5
Roll rate, p, deg/sec	Rate gyro	0.5
Yaw rate, r, deg/sec	Rate gyro	0.5
Right wingtip airspeed, $V_{R,M}$, knots	Tachometer	0.6
Left wingtip airspeed, $V_{L,M}$, knots	Tachometer	0.6
Pressure altitude, h, ft	Altimeter	39

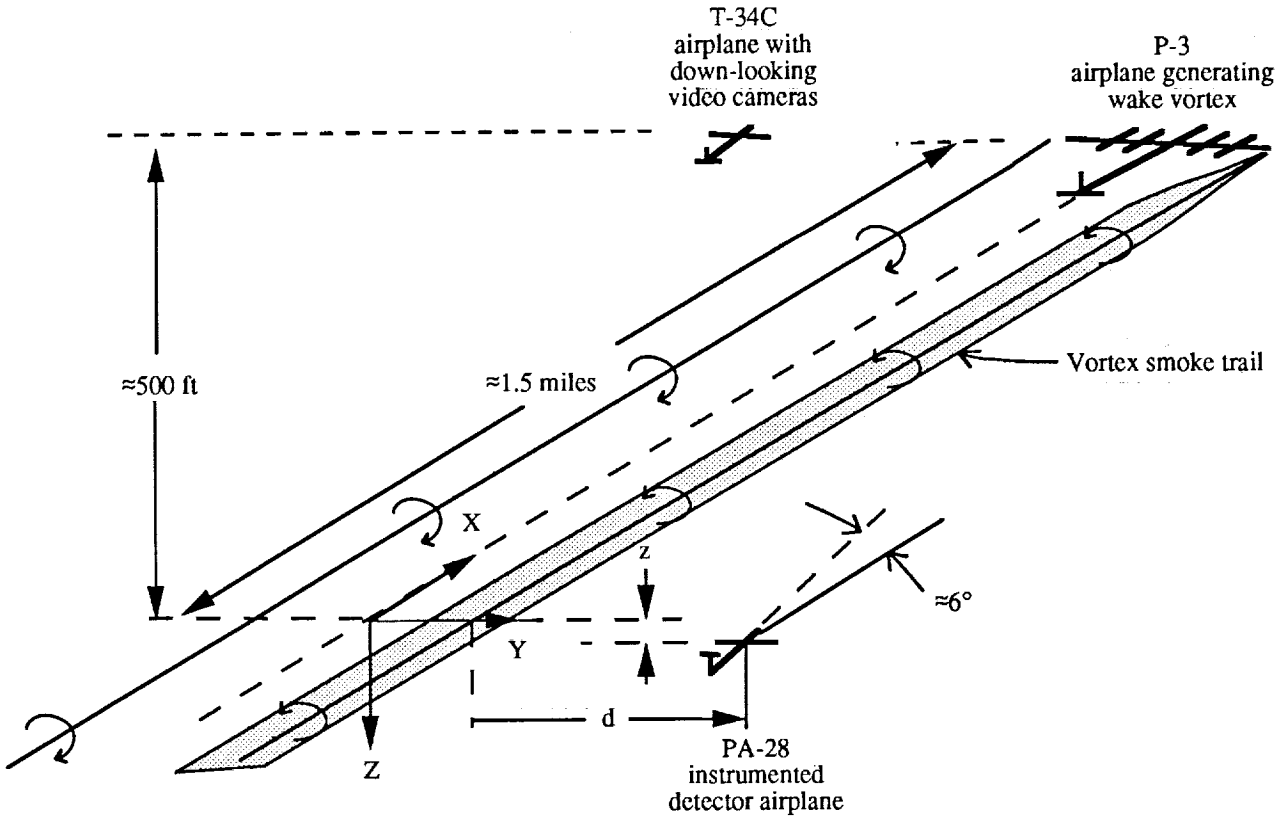

Figure 1. Wake vortex airborne detection experiment arrangement.

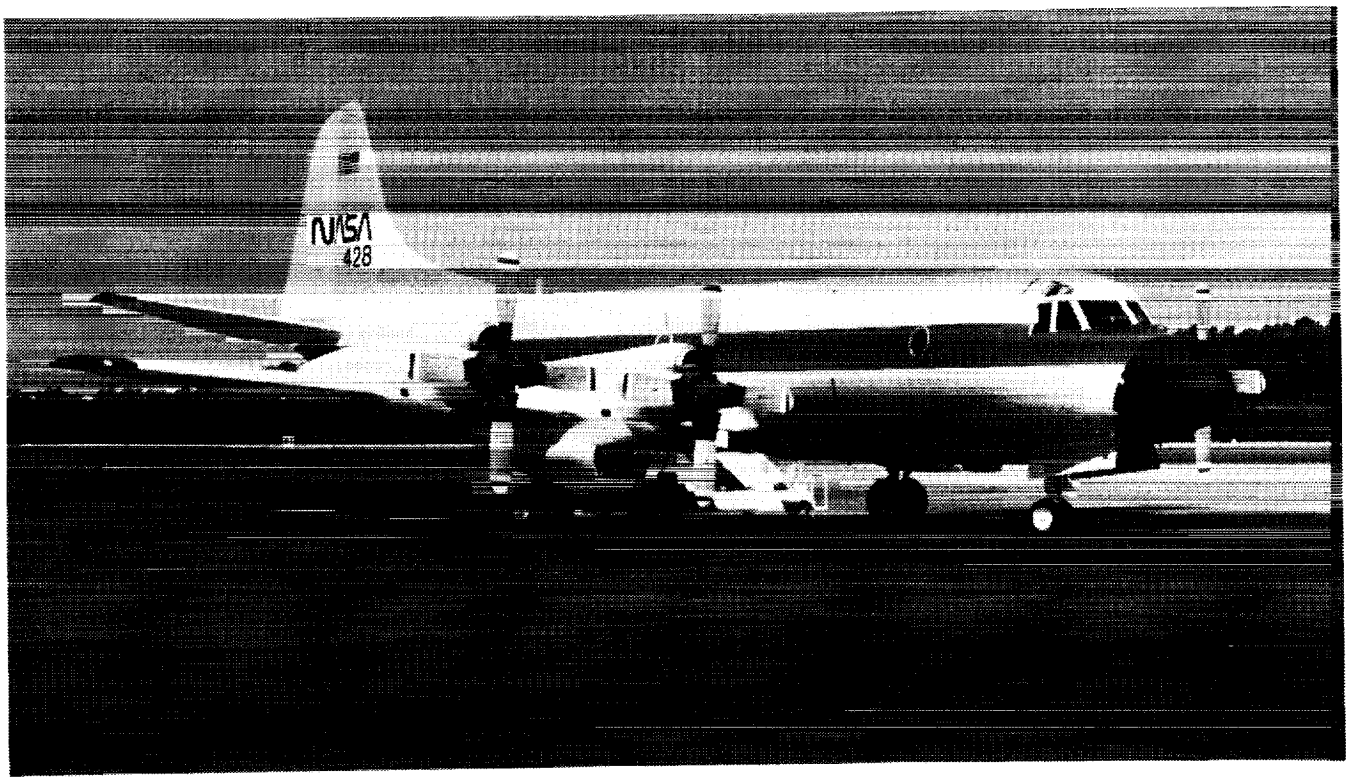

(a) On the ground.

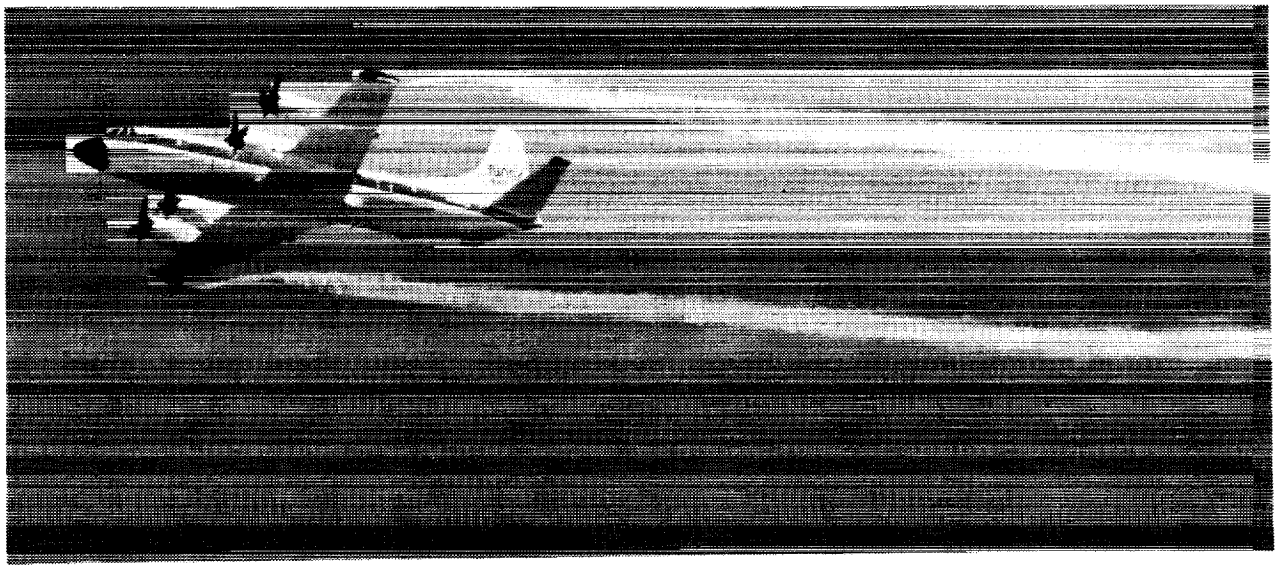

(b) In flight with wingtip vortices made visible with smoke.

Figure 2. P-3 airplane used to generate wake vortices.

L-91-63

Figure 3. PA-28 airplane used to detect wake vortices.

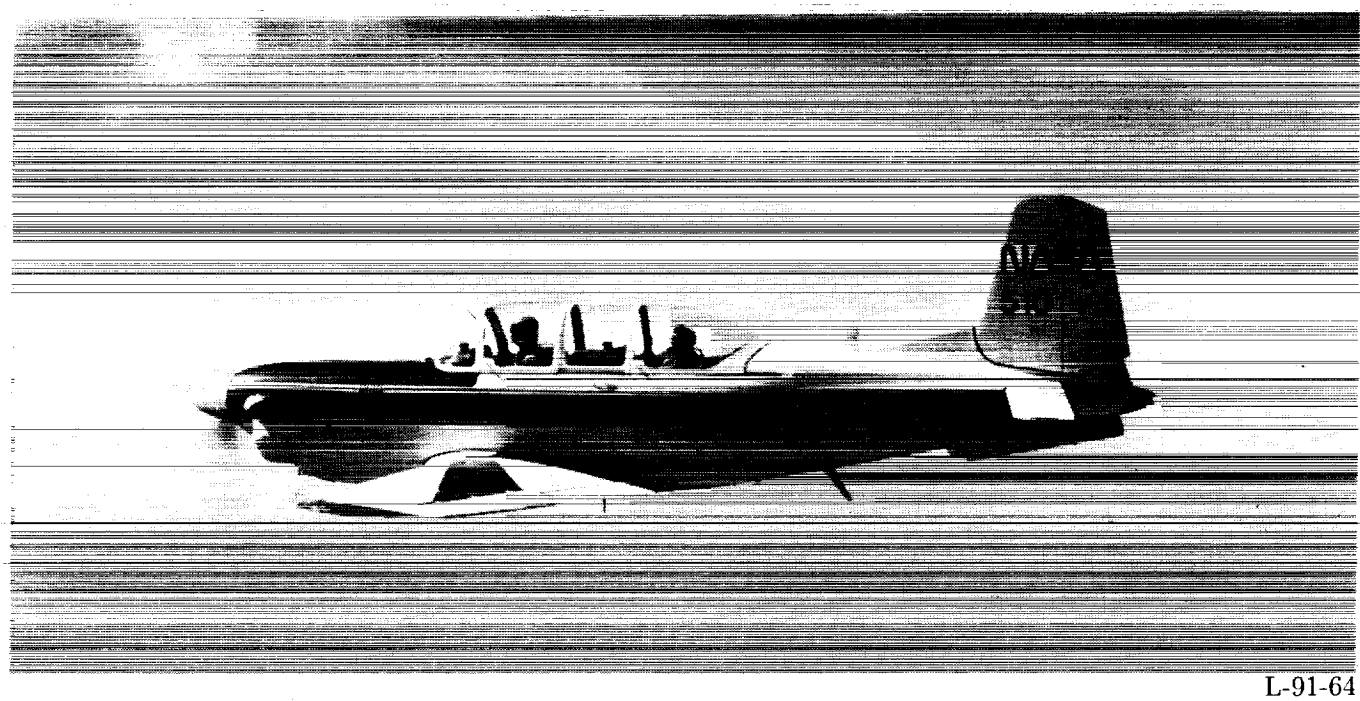

L-91-64

Figure 4. T-34C airplane used to photograph PA-28 airplane approaching smoke trails in wake vortices of the P-3 airplane.

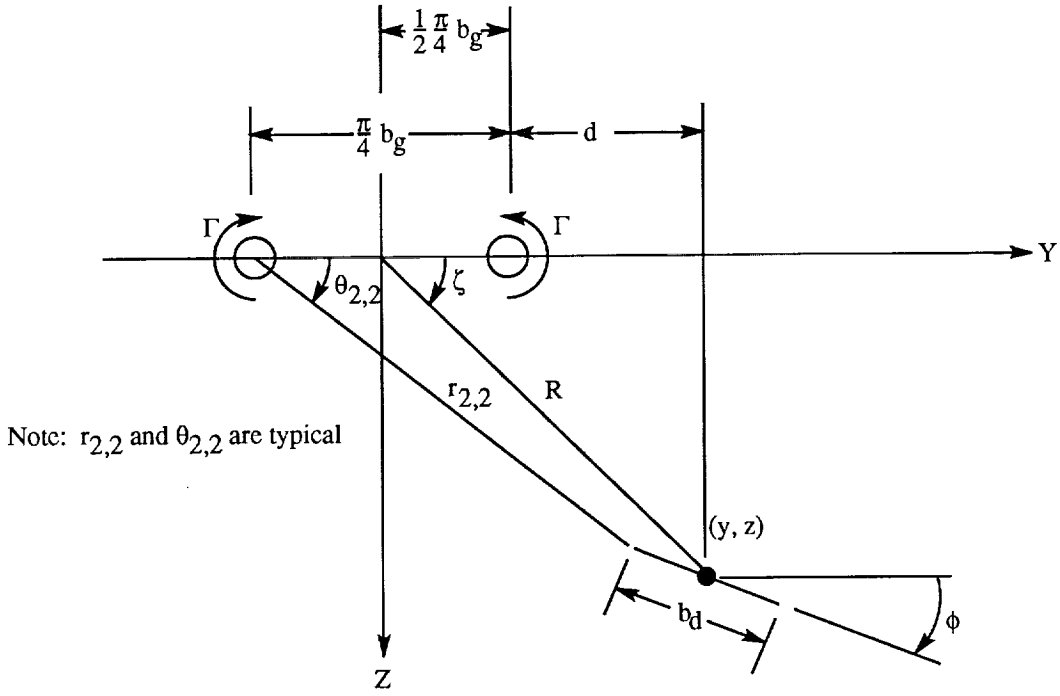

Figure 5. Geometry used in analysis.

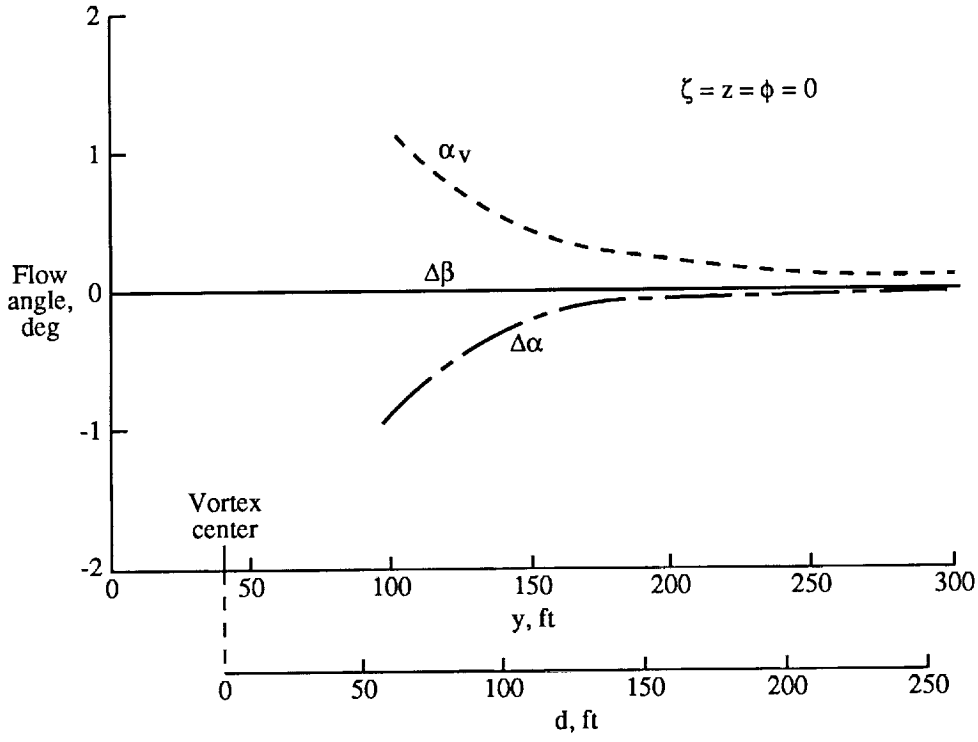

Figure 6. Effect of distance from vortices on flow angles when detecting airplane has a wings-level attitude and is in the plane of the vortices.

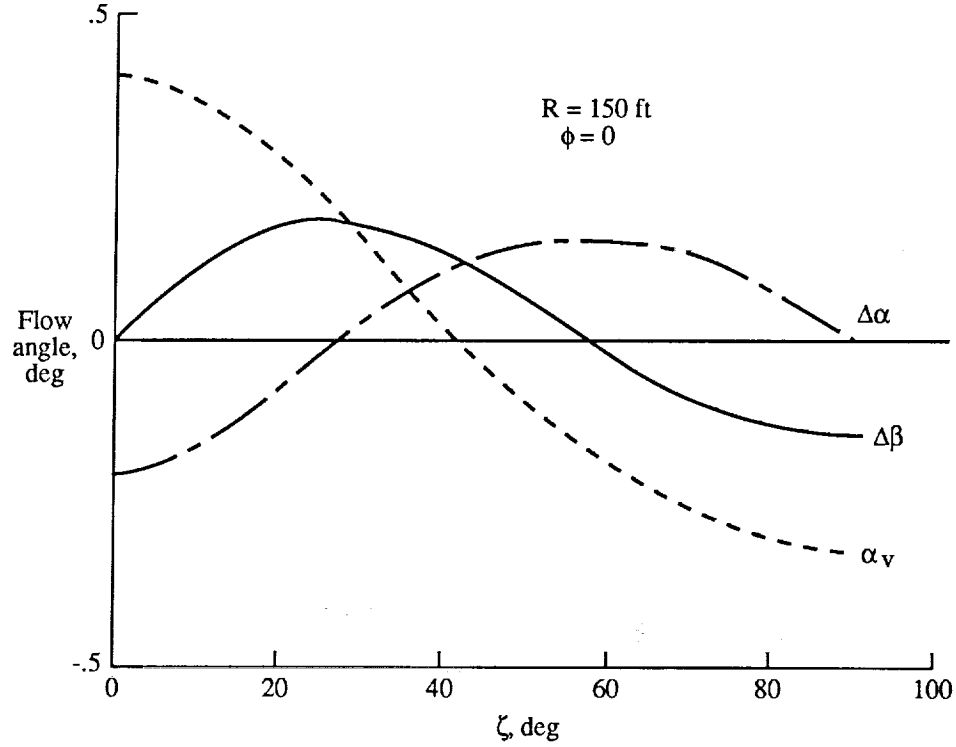

Figure 7. Effect of angular position from center of vortex pair.

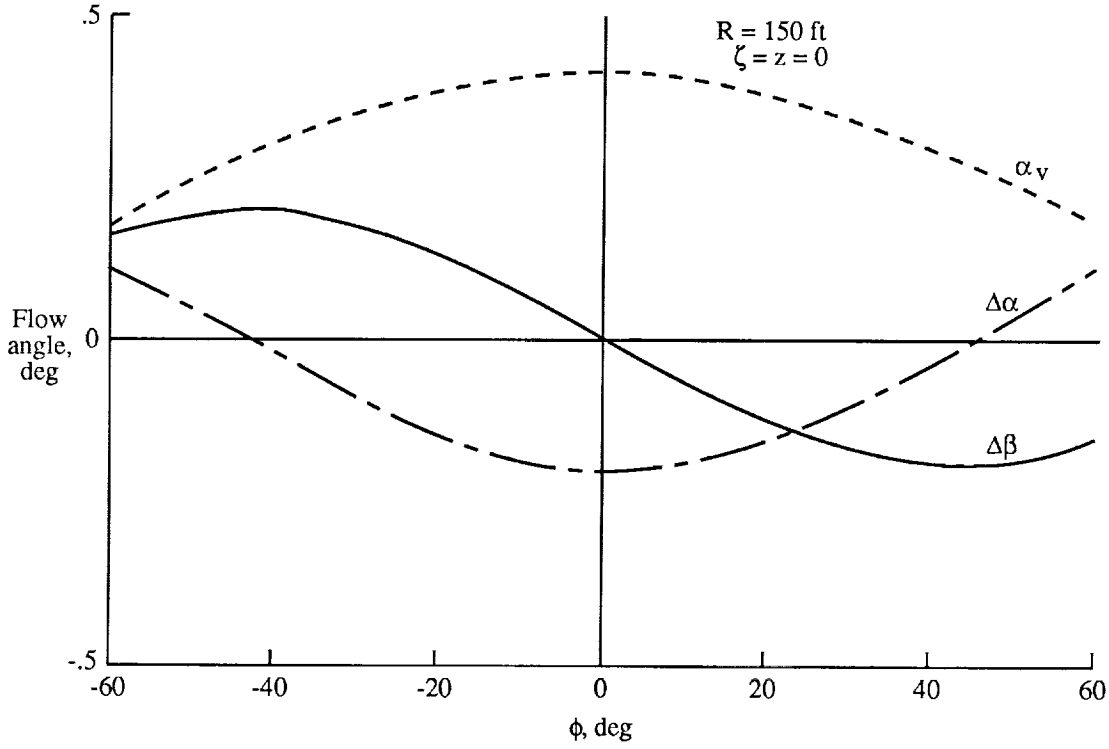

Figure 8. Effect of roll attitude of detecting airplane on flow angles.

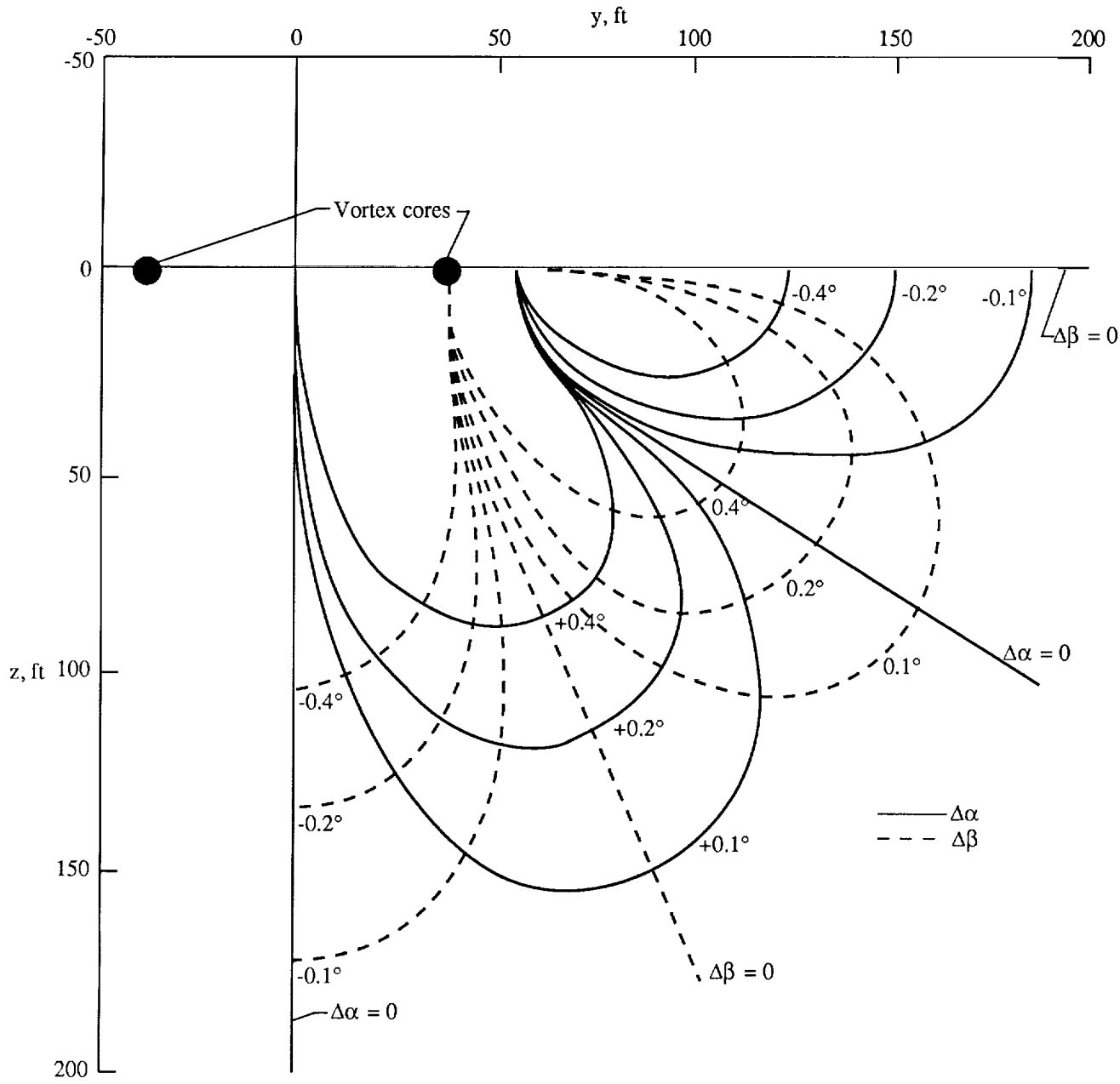

Figure 9. Contours of constant differential flow angles with wings level ($\phi = 0$).

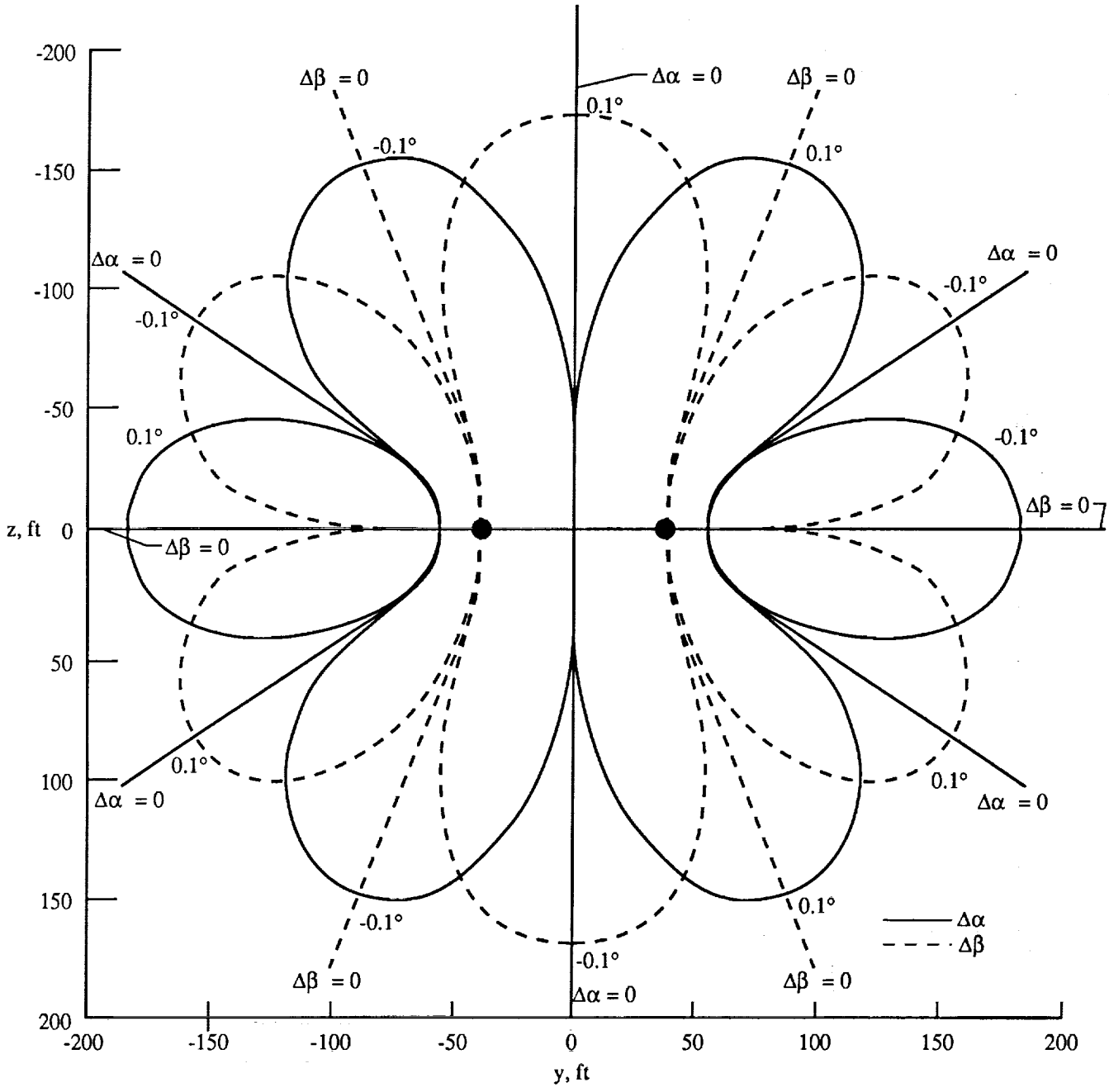

Figure 10. Contours of equal absolute values of differential flow angles with wings level ($\phi = 0$).

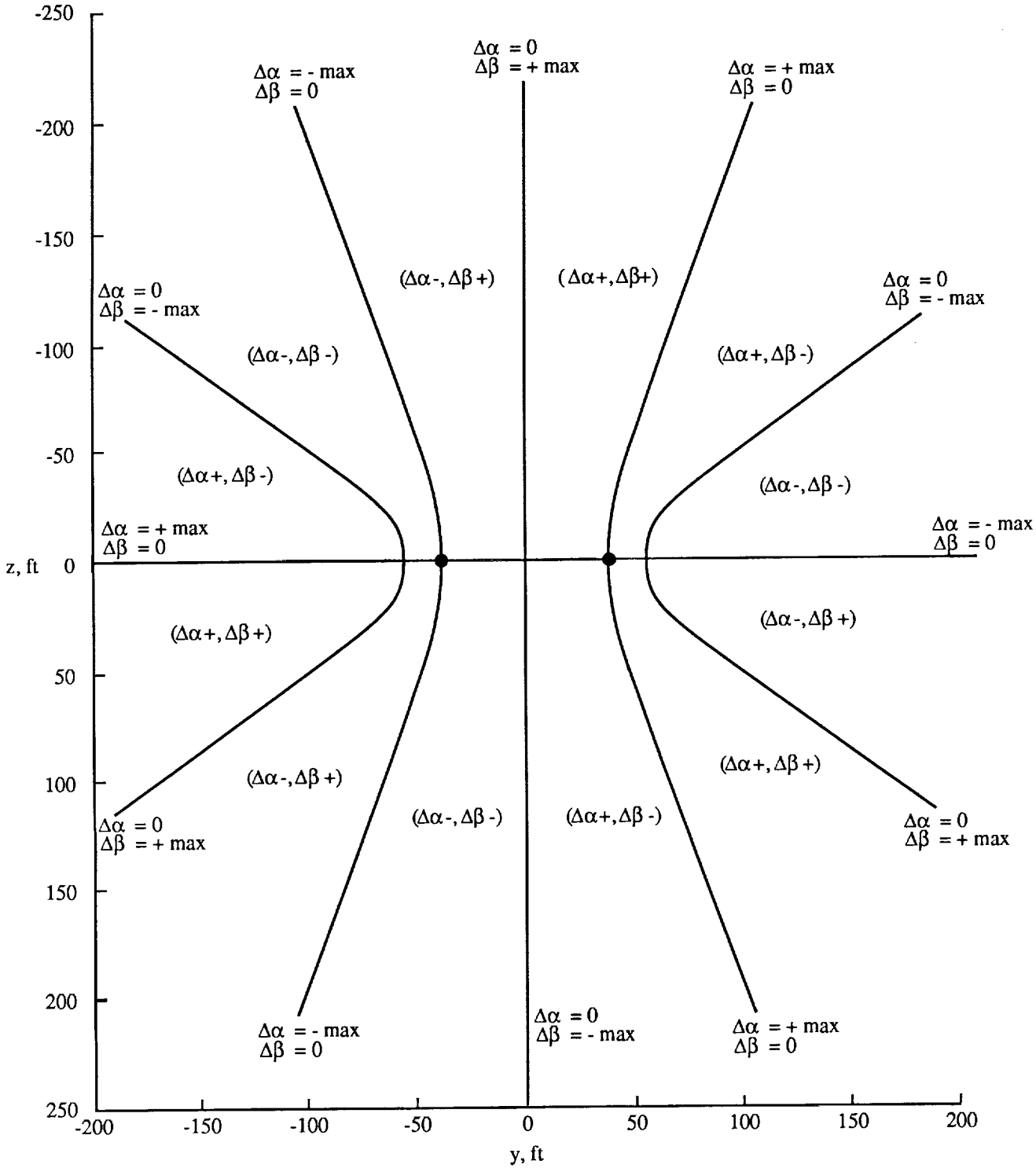

Figure 11. Twelve sectors defined by combination of signs on differential flow angles.

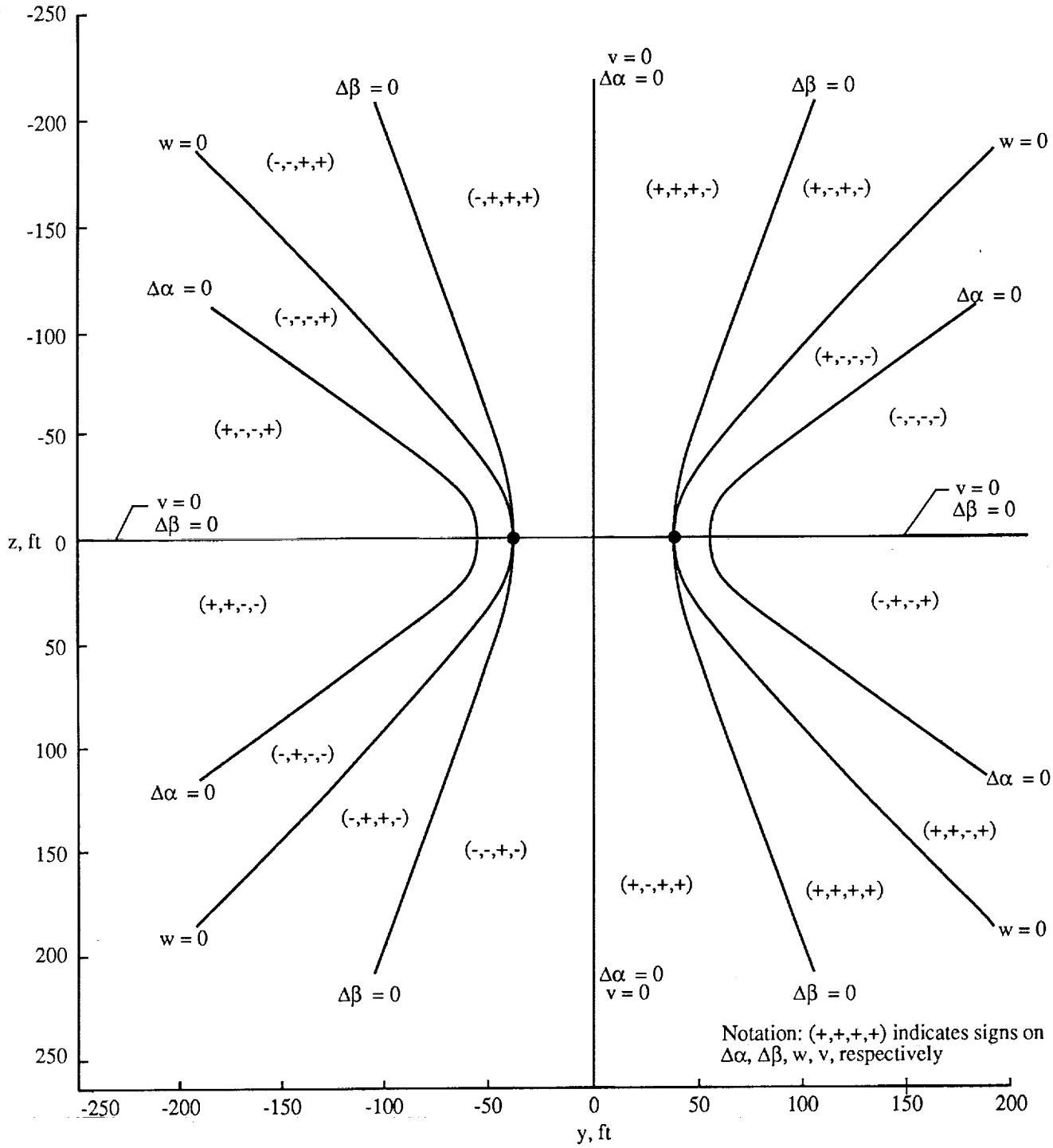

Figure 12. Sixteen sectors defined by combination of signs on differential flow angles and vortex velocity components ($\phi = 0$).

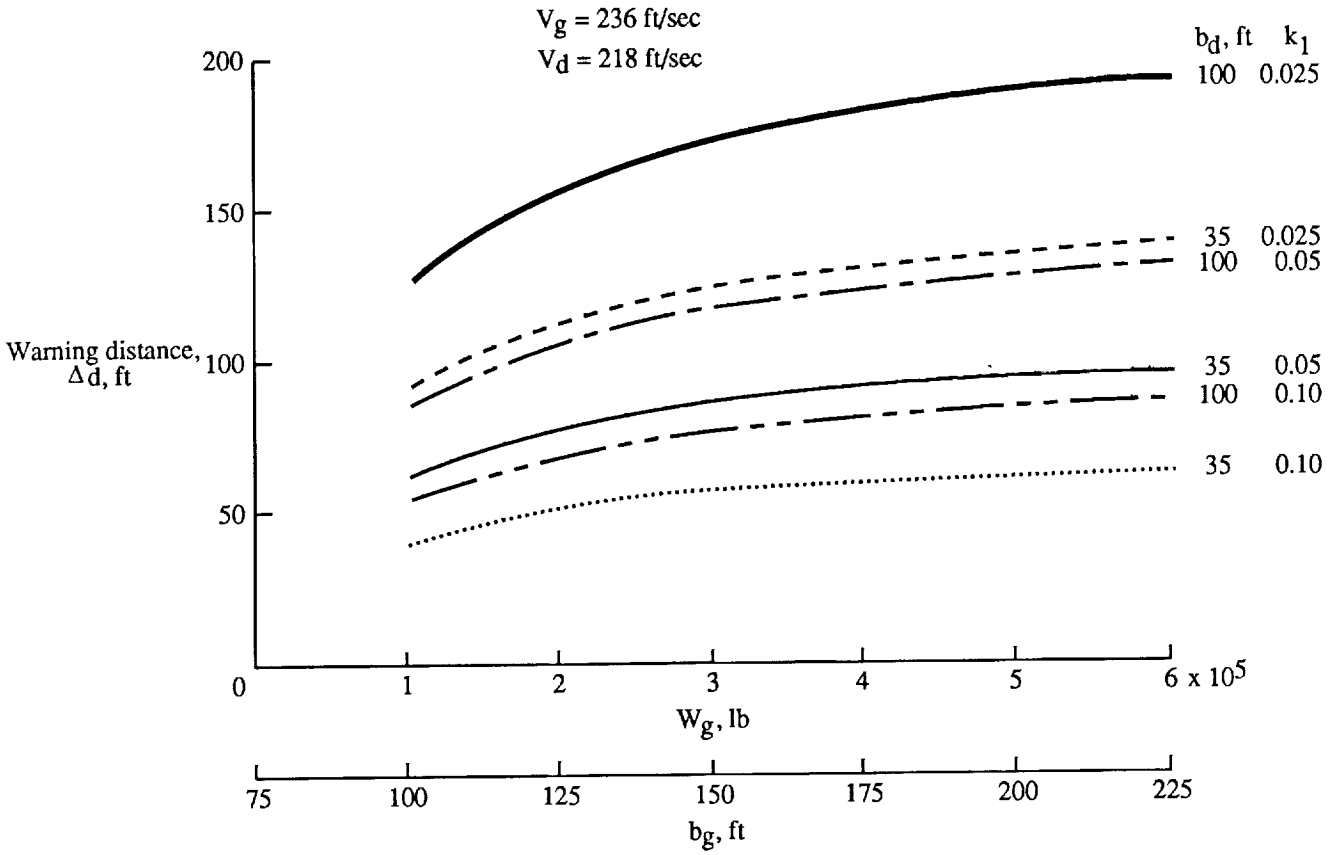

Figure 13. Theoretical warning distance for assumed configurations and detection thresholds k_1 with $k_2 = 1.0$.

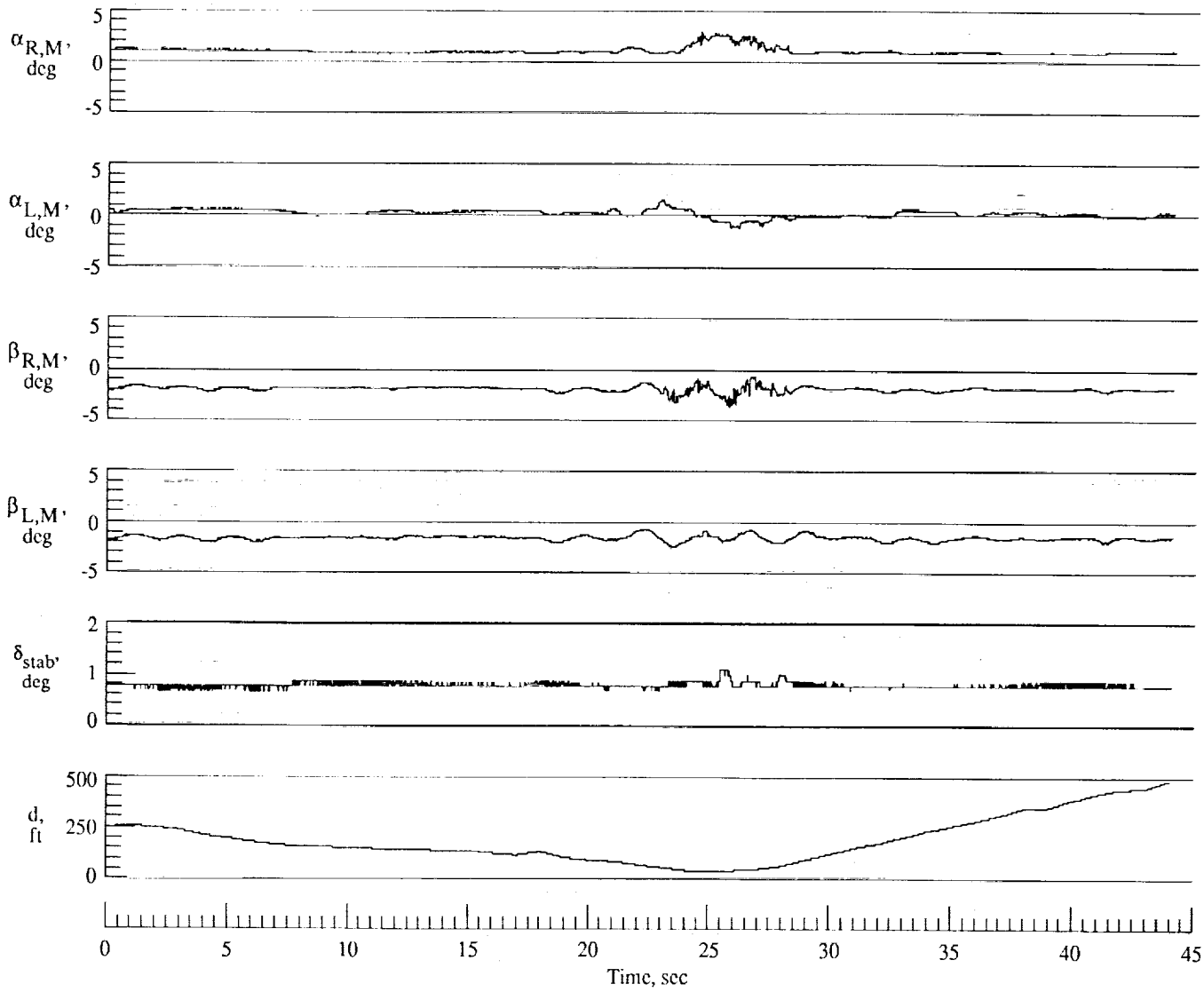

(a) Flow angles, stabilator position, and horizontal distance to nearest vortex.

Figure 14. Unprocessed data with flaps retracted on vortex-generating airplane.

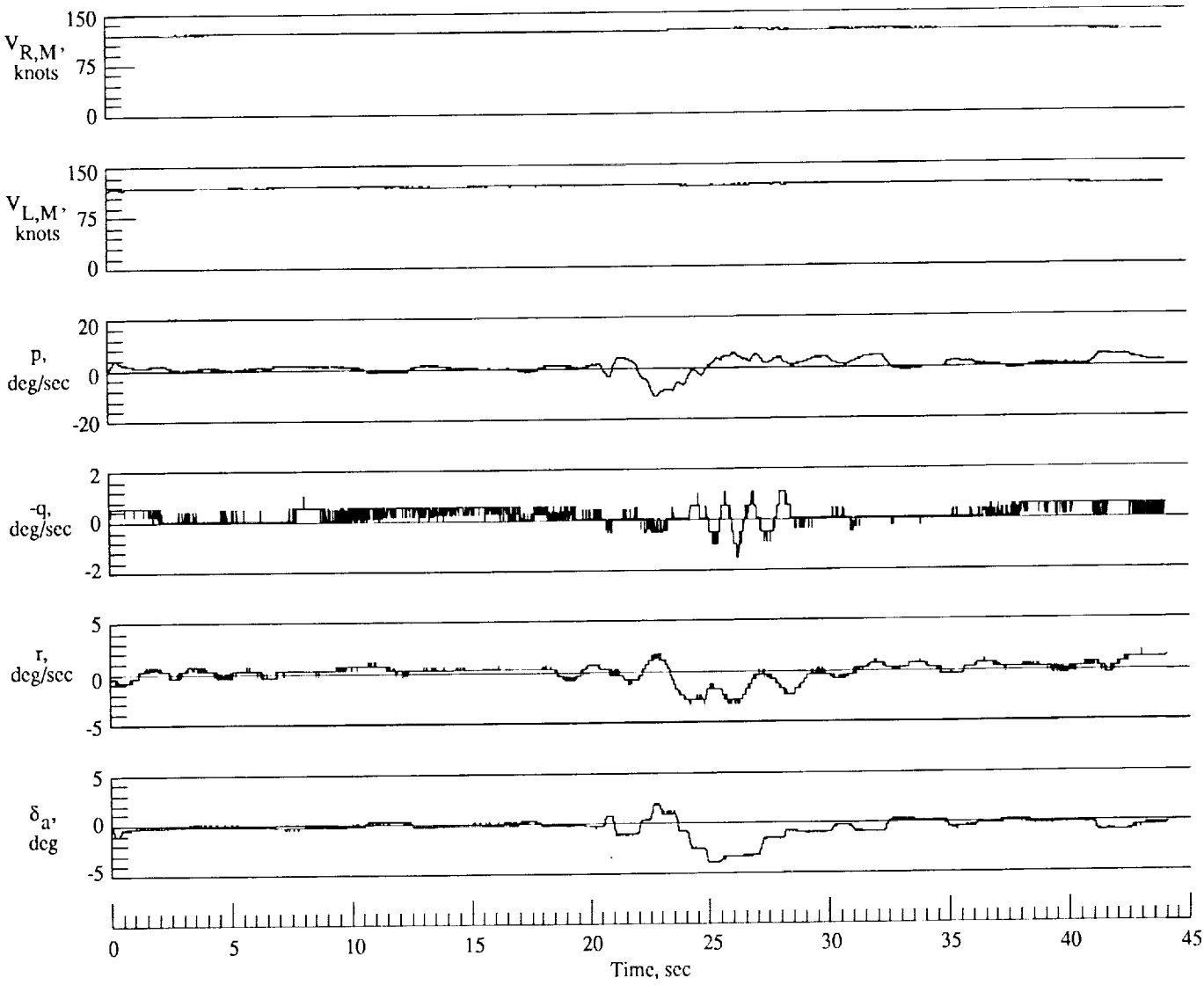

(b) Airspeed, angular rates, and aileron position.

Figure 14. Continued.

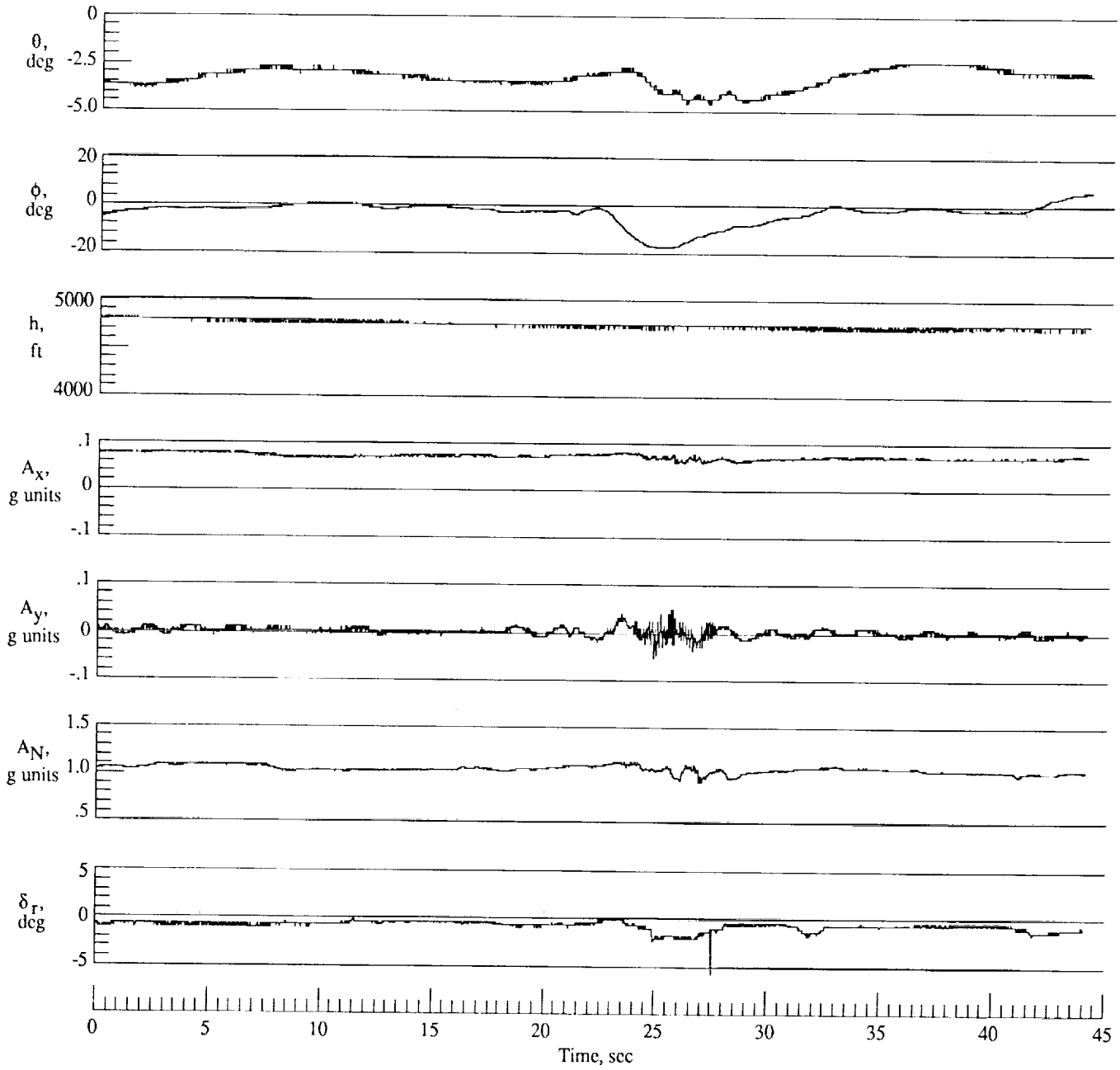

(c) Attitude, altitude, linear accelerations, and rudder position.

Figure 14. Concluded.

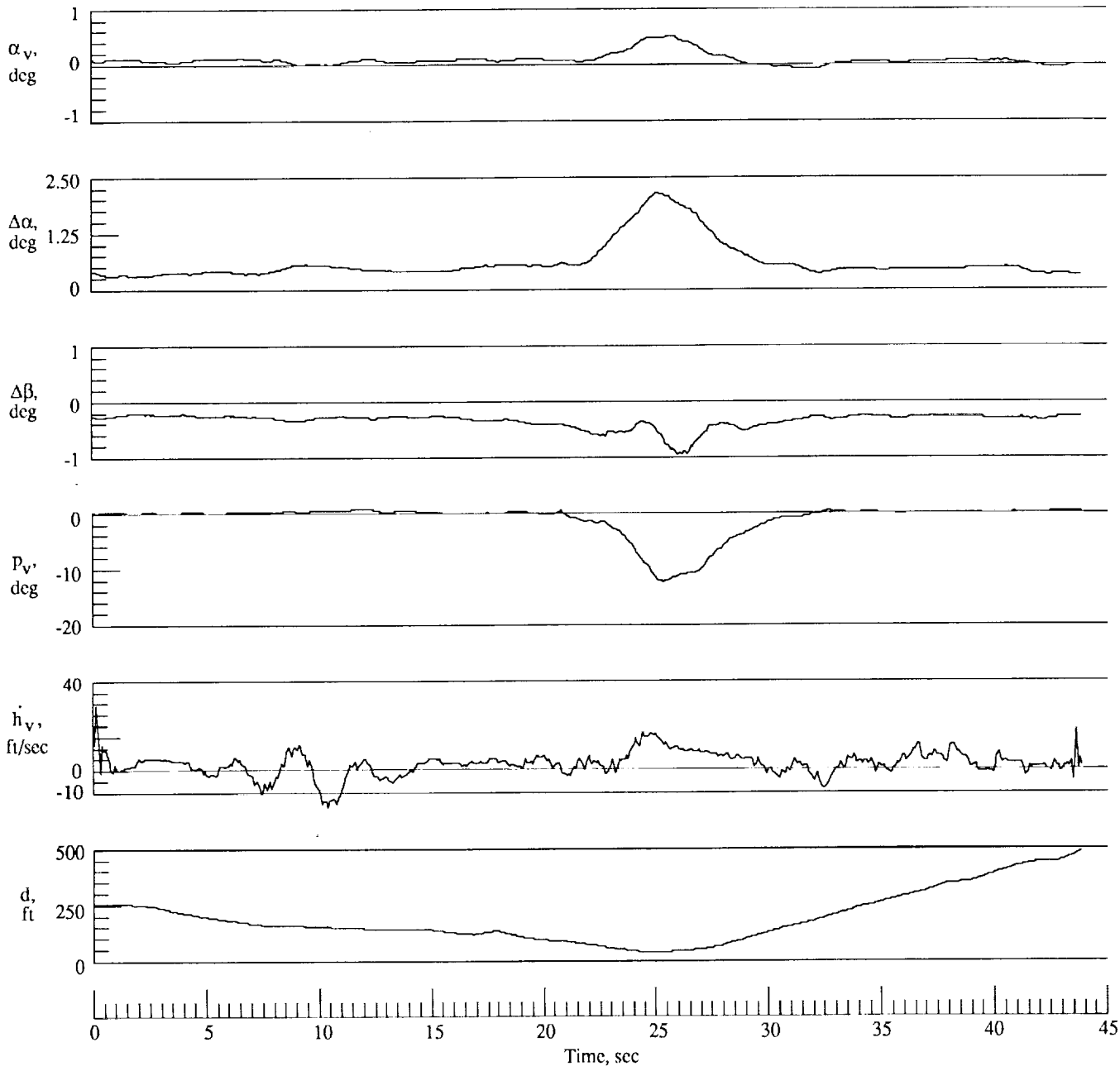

Figure 15. Processed data with flaps retracted on vortex-generating airplane (test 2-10, run 1, ref. 3).

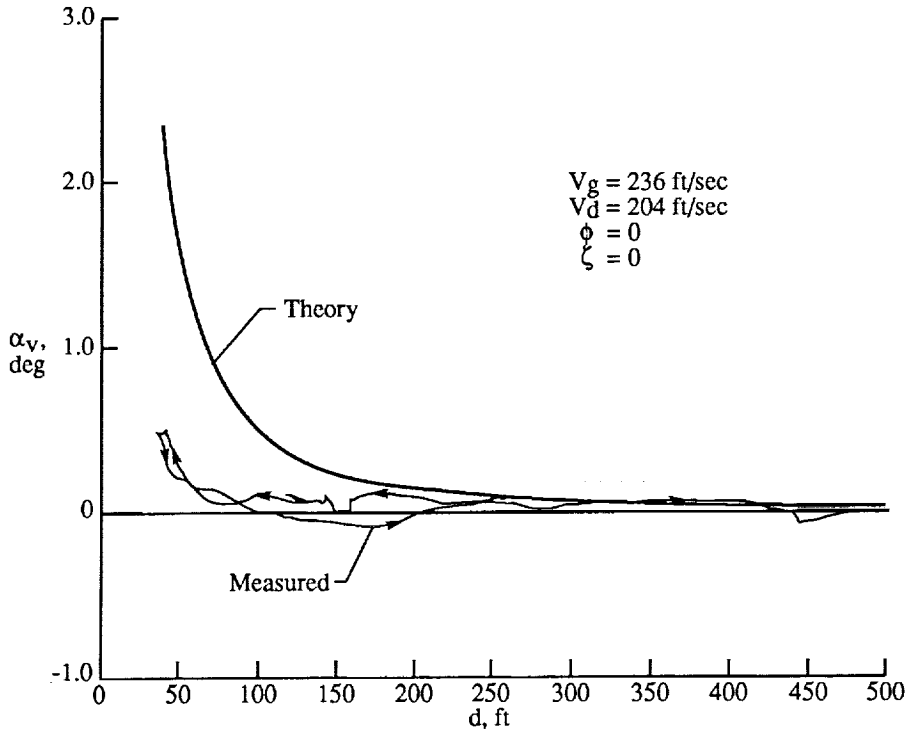

(a) Flaps retracted on vortex-generating airplane (test 2-10, run 1, ref. 3).

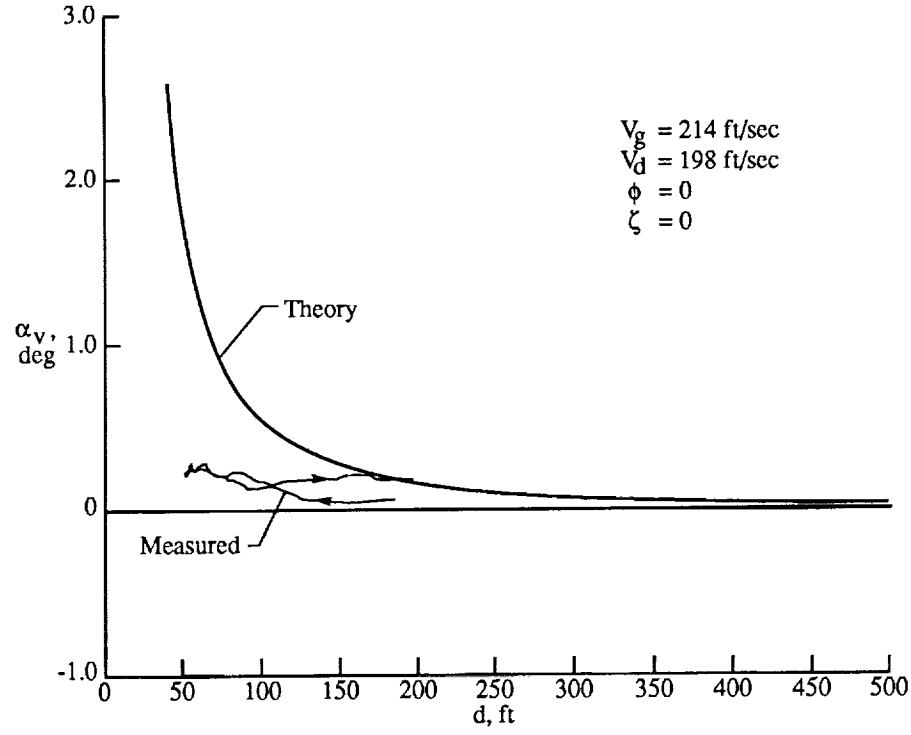

(b) Flaps extended on vortex-generating airplane (test 2-10, run 10, ref. 3).

Figure 16. Effect of vortex flow field on angle of attack.

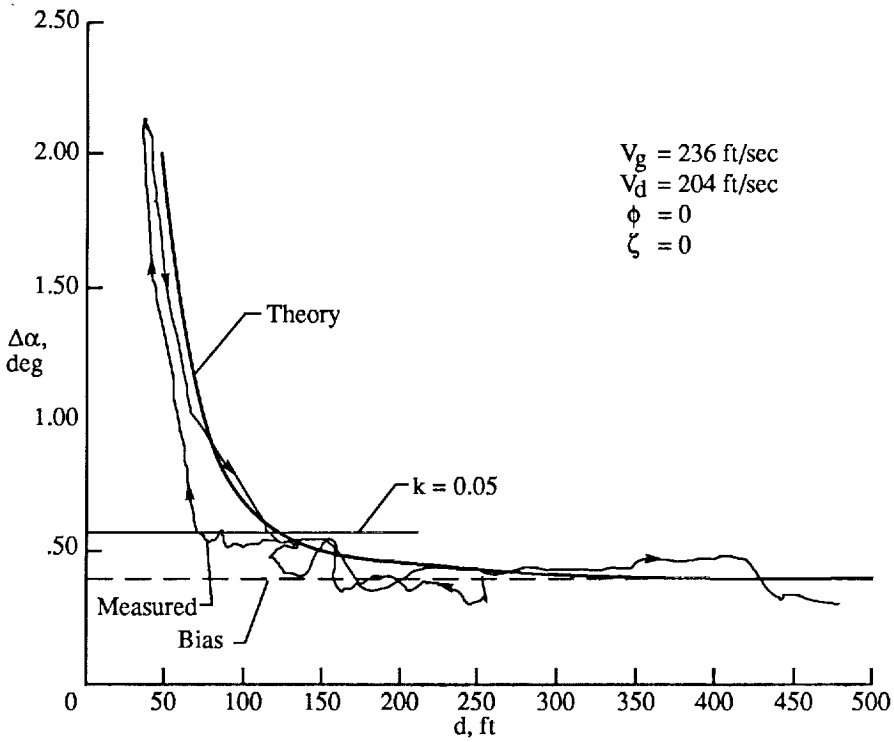

(a) Flaps retracted on vortex-generating airplane (test 2-10, run 1, ref. 3).

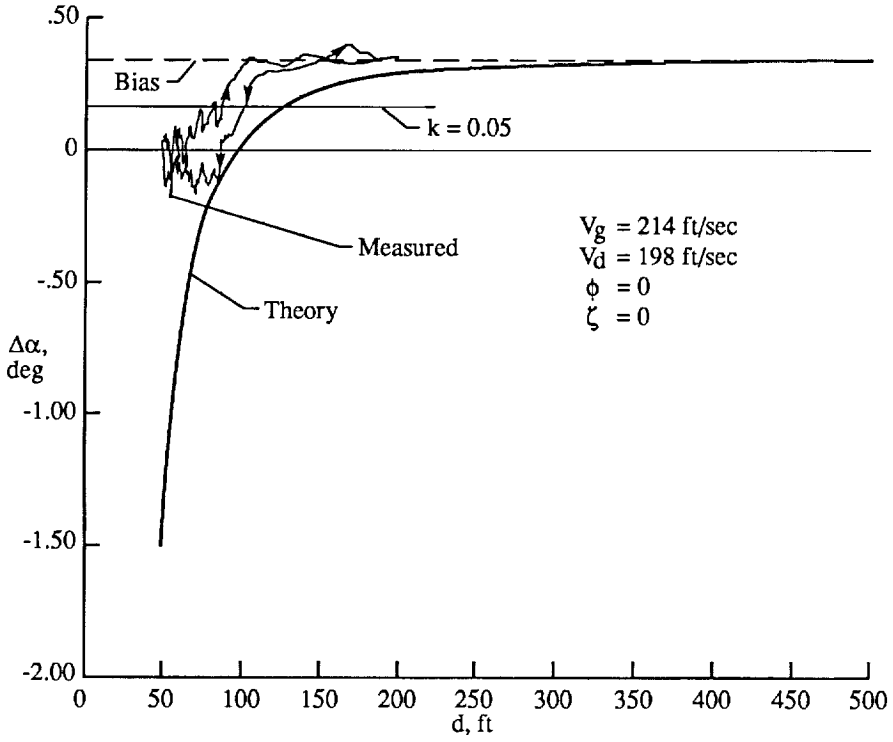

(b) Flaps extended on vortex-generating airplane (test 2-10, run 10, ref. 3).

Figure 17. Effect of vortex flow field on differential angle of attack.

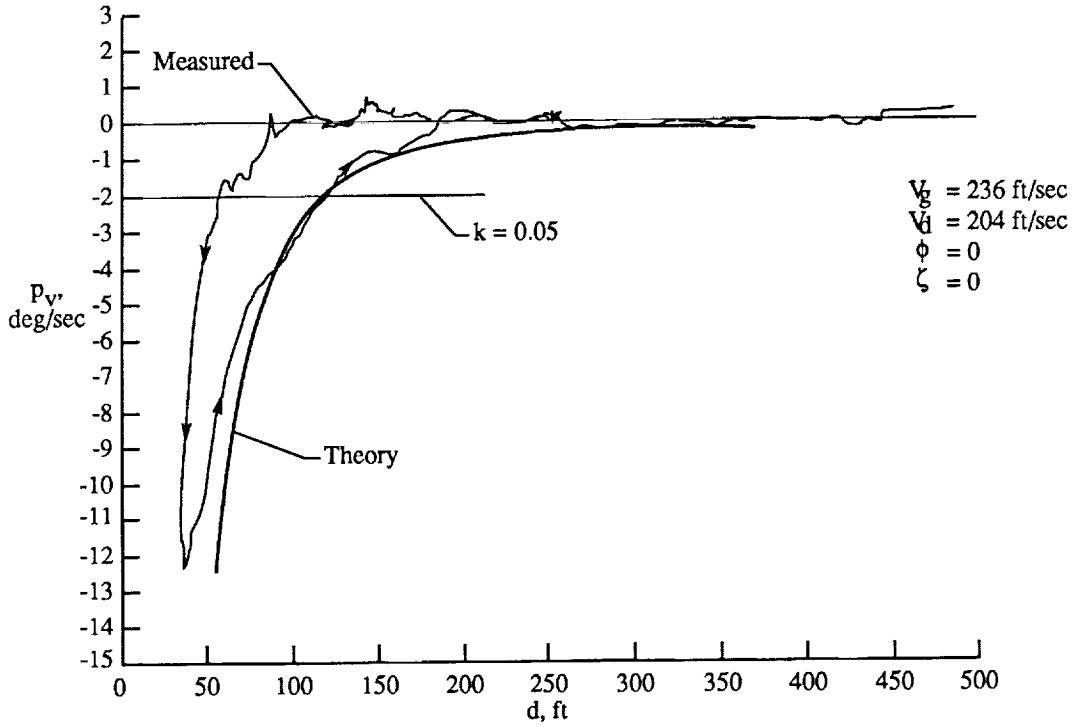

(a) Flaps retracted on vortex-generating airplane (test 2-10, run 1, ref. 3).

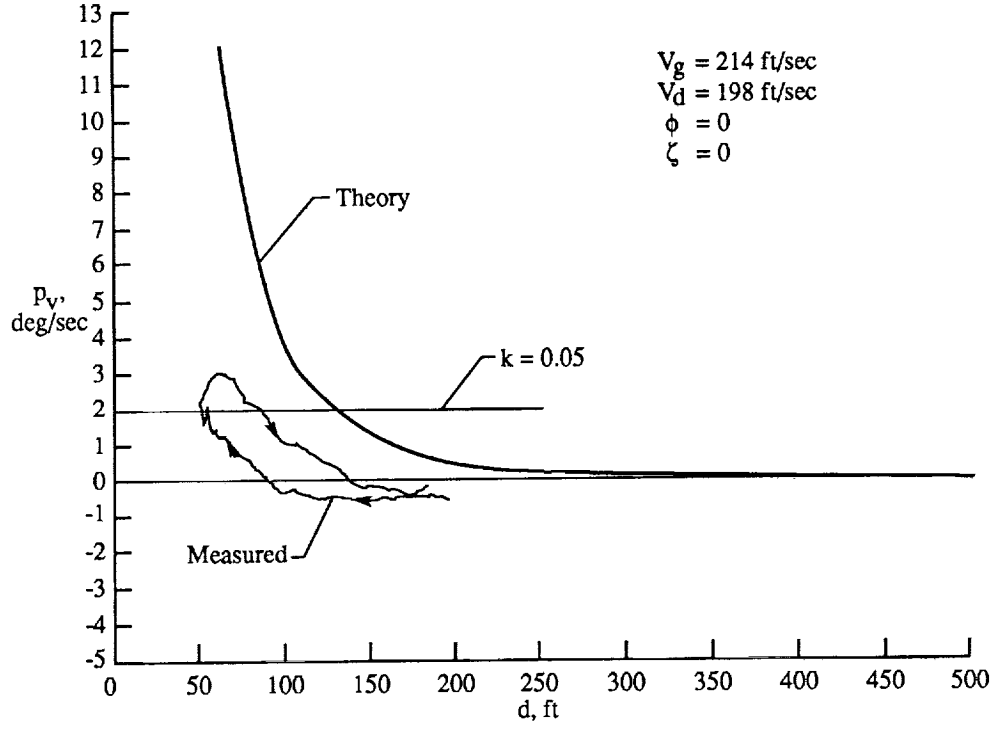

(b) Flaps extended on vortex-generating airplane (test 2-10, run 10, ref. 3).

Figure 18. Effect of vortex flow field on vortex roll rate parameter.

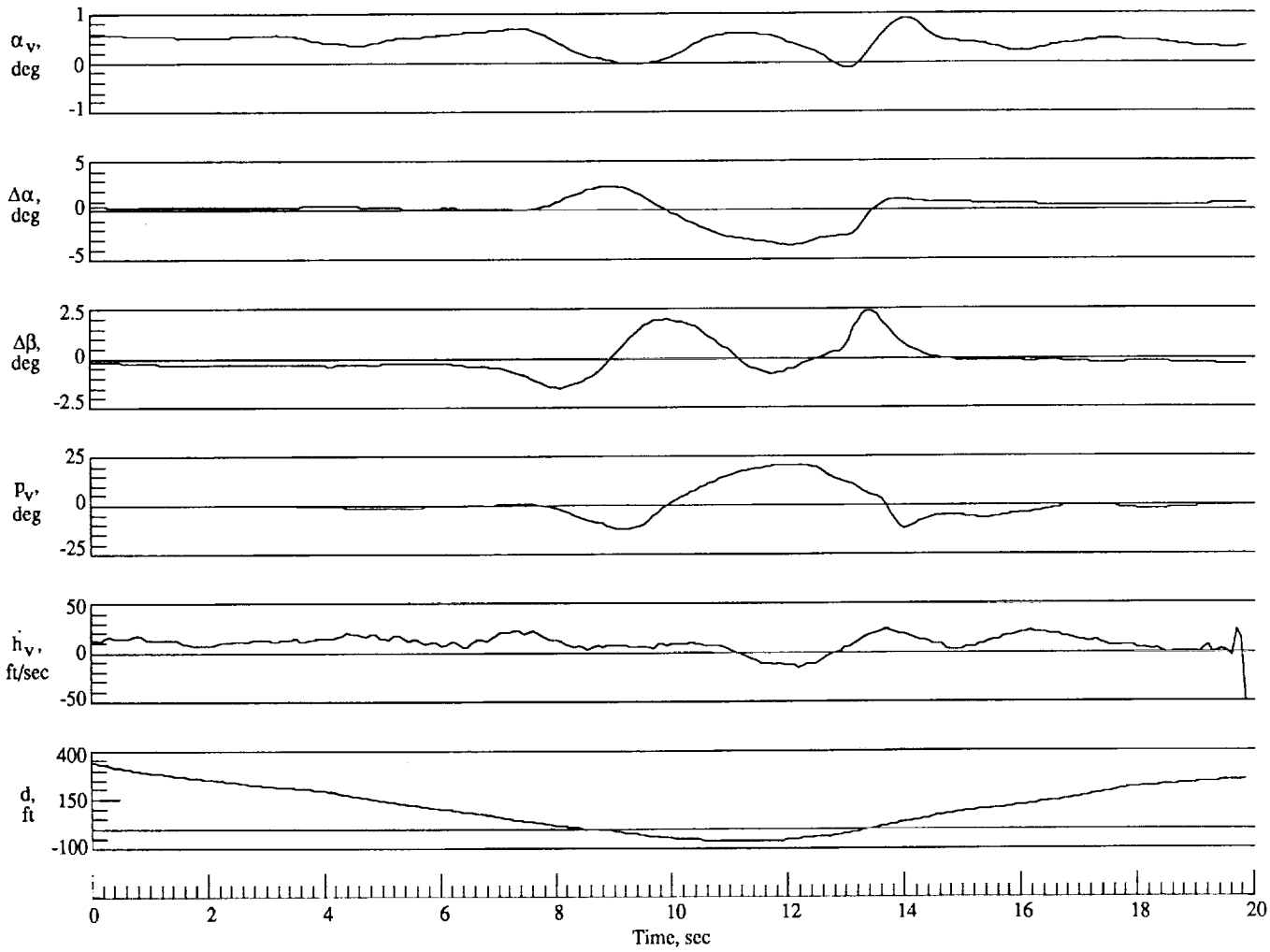

Figure 19. Processed data (PA-28 detector airplane approached vortex off its left wing and then flew over the top of the vortex).

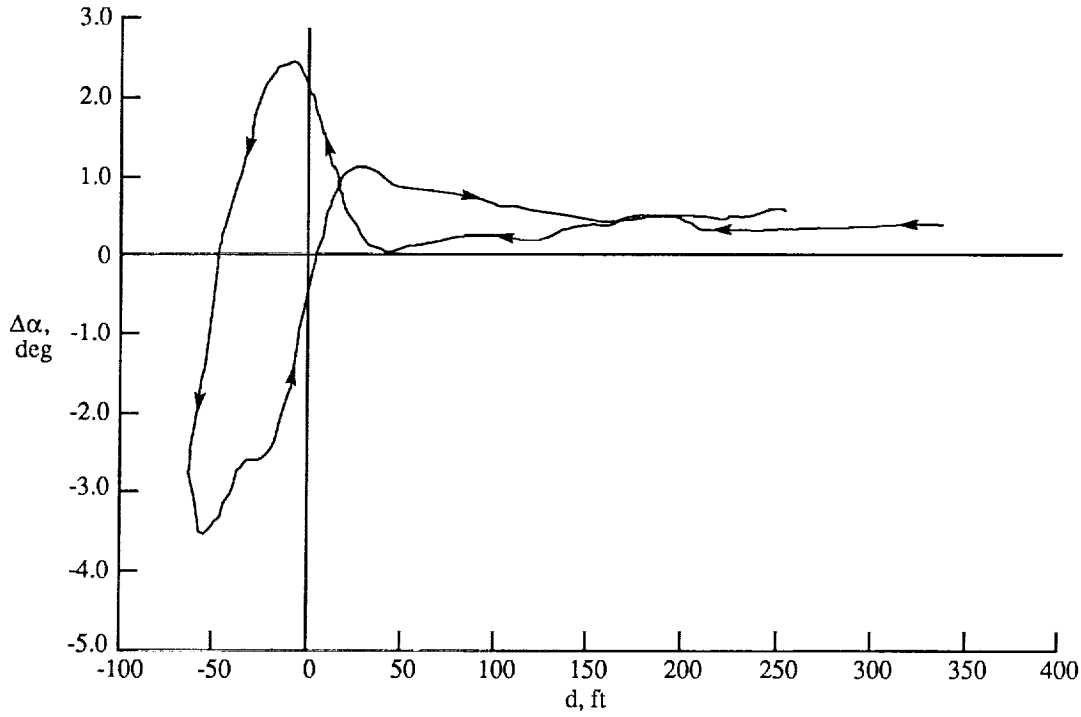

(a) Differential angle of attack.

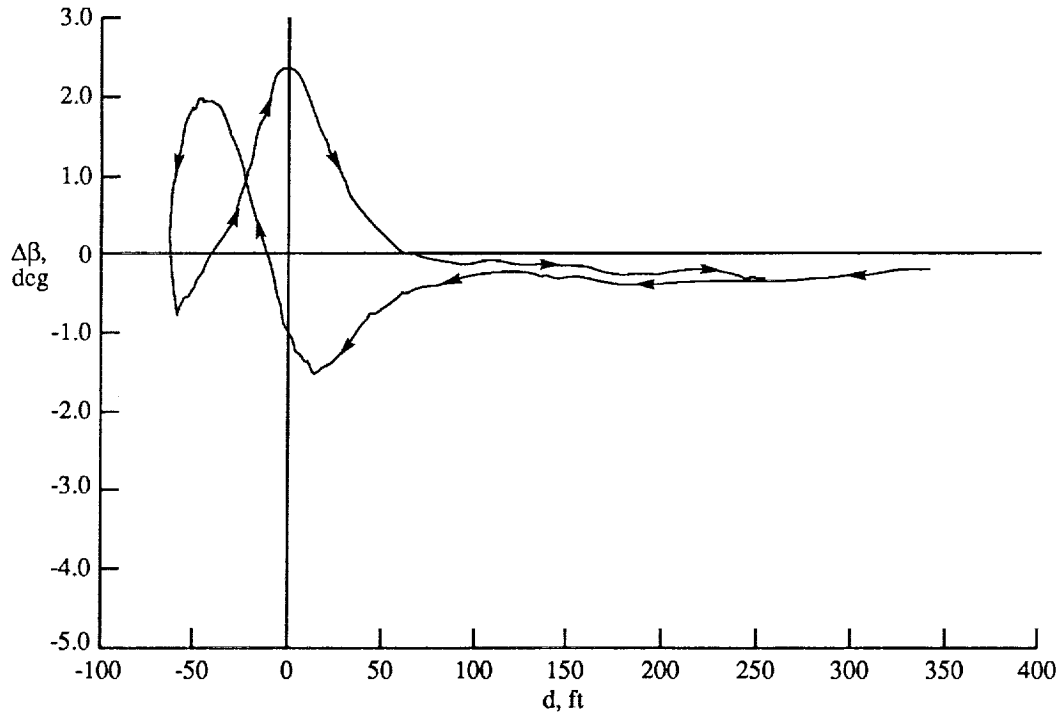

(b) Differential angle of sideslip.

Figure 20. Effect of horizontal distance on differential flow angles (PA-28 detector airplane approached vortex off its left wing and then flew over the top of the vortex).

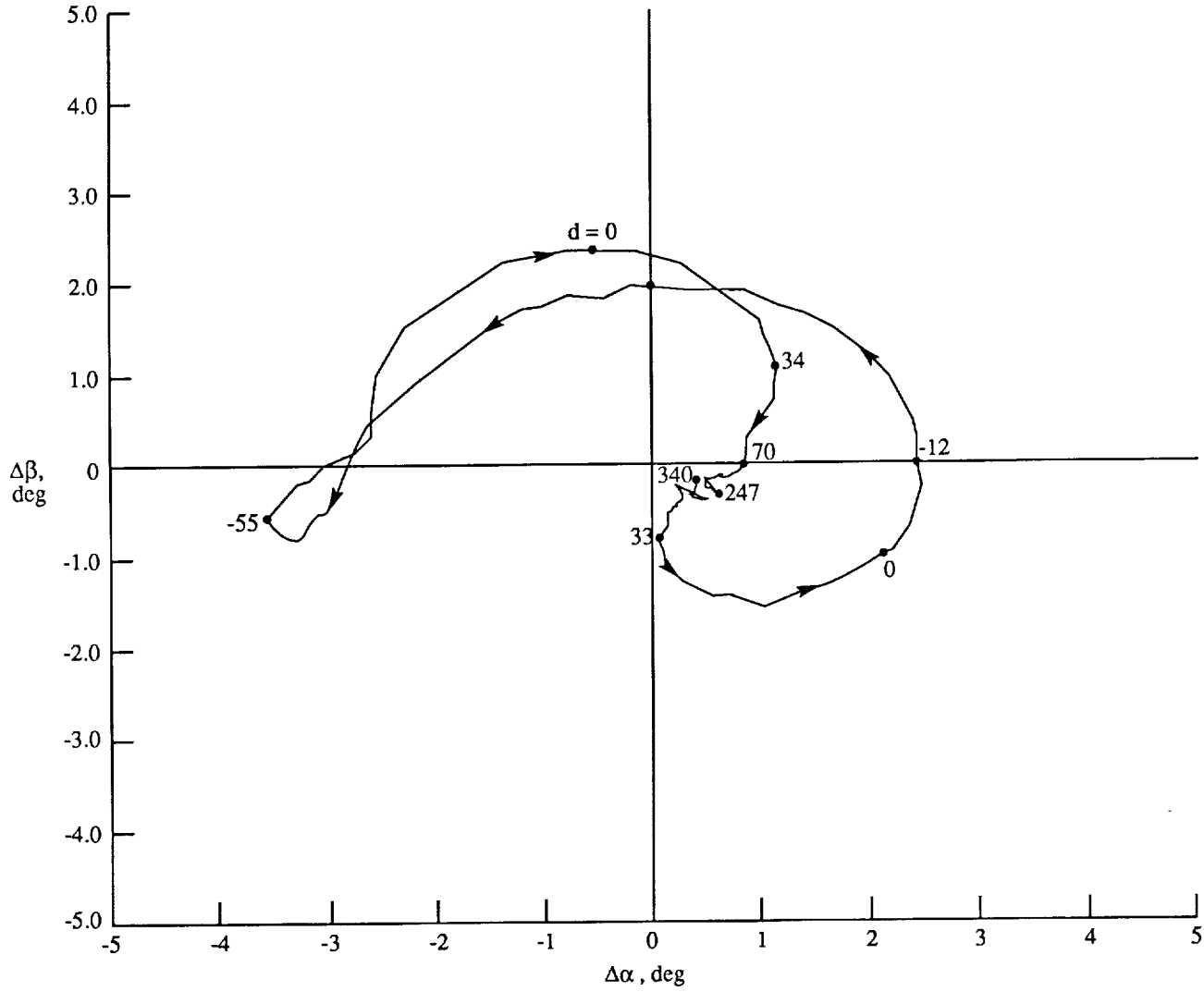

Figure 21. Cross plot of differential flow angles (PA-28 detector airplane approached vortex off its left wing and then flew over the top of the vortex).

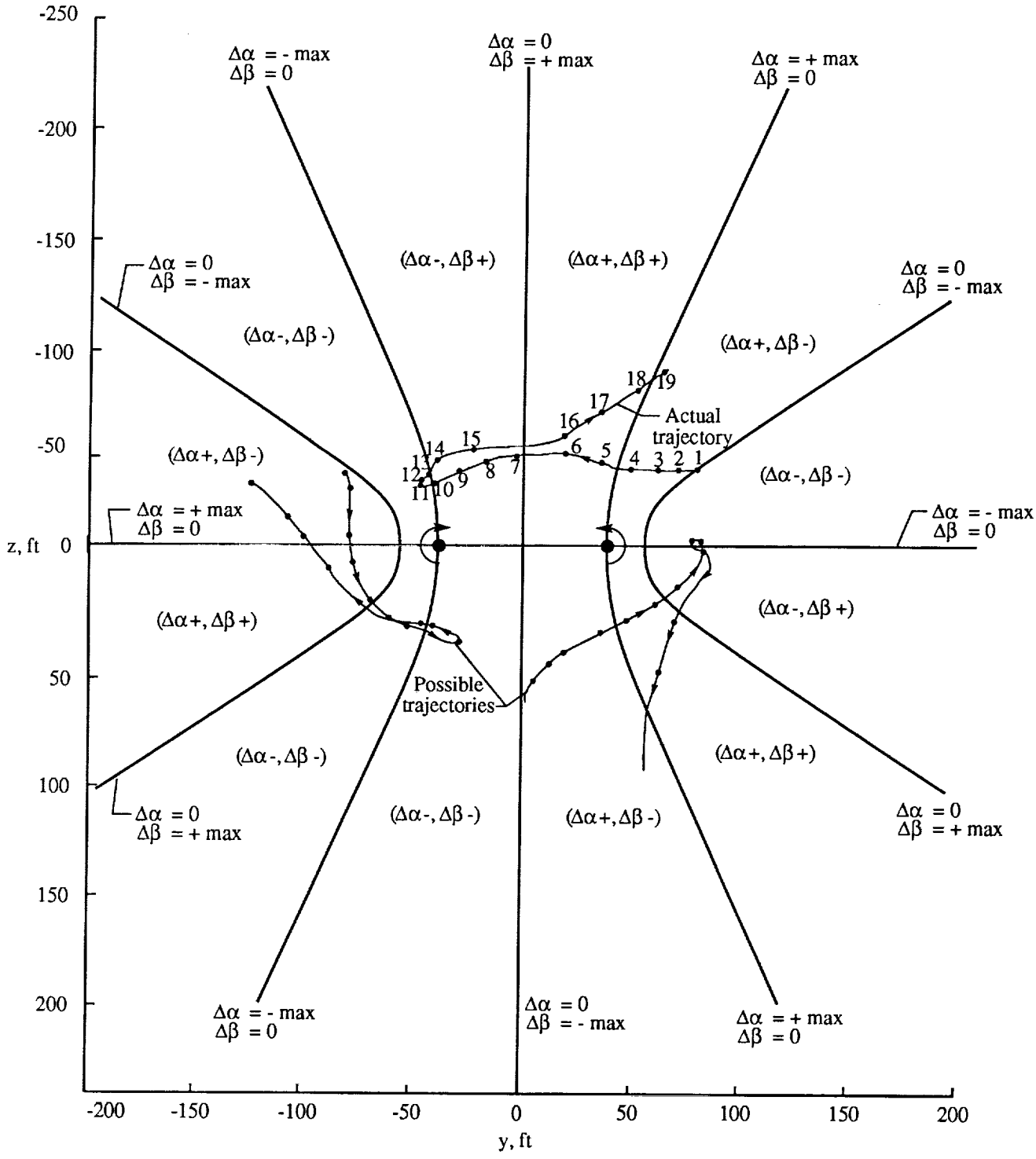

Figure 22. Trajectories reconstructed from angular flow measurements shown in figure 19 and video data.

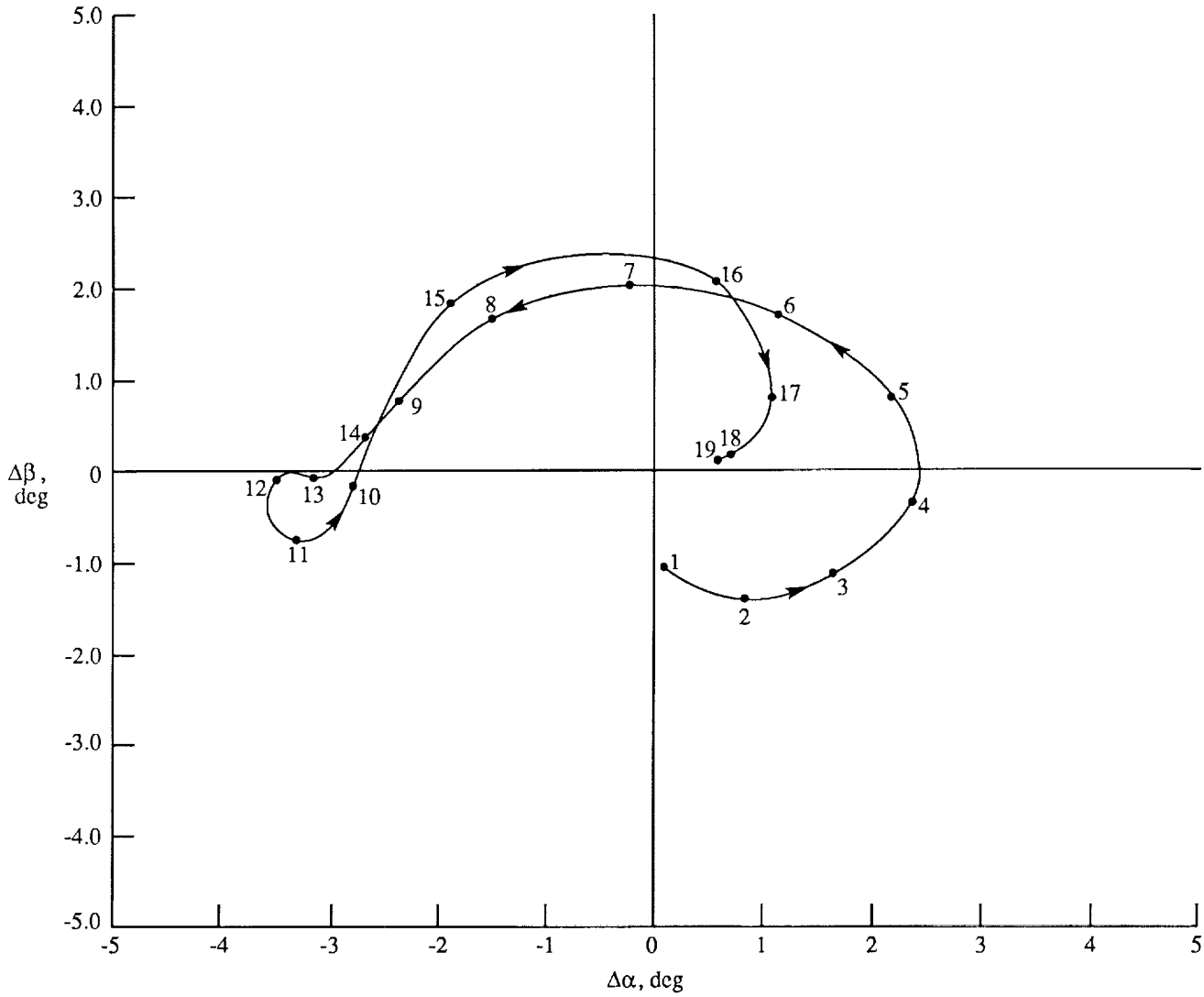

Figure 23. Theoretical cross plot of flow angles for trajectories shown in figure 20. Numbers on curve correspond to numbers on trajectory in figure 22.

REPORT DOCUMENTATION PAGE

Form Approved
OMB No. 0704-0188

1. AGENCY USE ONLY *(Leave blank)*	2. REPORT DATE	3. REPORT TYPE AND DATES COVERED
	November 1991	Technical Paper

4. TITLE AND SUBTITLE
A Comparison of Airborne Wake Vortex Detection Measurements With Values Predicted From Potential Theory

5. FUNDING NUMBERS
WU 505-68-10-01

6. AUTHOR(S)
Eric C. Stewart

7. PERFORMING ORGANIZATION NAME(S) AND ADDRESS(ES)
NASA Langley Research Center
Hampton, VA 23665-5225

8. PERFORMING ORGANIZATION REPORT NUMBER
L-16899

9. SPONSORING/MONITORING AGENCY NAME(S) AND ADDRESS(ES)
National Aeronautics and Space Administration
Washington, DC 20546-0001

10. SPONSORING/MONITORING AGENCY REPORT NUMBER
NASA TP-3125

11. SUPPLEMENTARY NOTES

12a. DISTRIBUTION/AVAILABILITY STATEMENT
Unclassified Unlimited

Subject Category 03

12b. DISTRIBUTION CODE

13. ABSTRACT *(Maximum 200 words)*

An analysis of flight measurements made near a wake vortex was conducted to explore the feasibility of providing a pilot with useful wake-avoidance information. The measurements were made with relatively low-cost flow and motion sensors on a light airplane flying near the wake vortex of a turboprop airplane weighing approximately 90 000 lb. Algorithms were developed which removed the response of the airplane to control inputs from the total airplane response and produced parameters which were due solely to the flow field of the vortex. These parameters were compared with values predicted by potential theory. The results indicated that the presence of the vortex could be detected by a combination of parameters derived from the simple sensors. However, the location and strength of the vortex cannot be determined without additional and more accurate sensors.

14. SUBJECT TERMS	15. NUMBER OF PAGES
Wake vortex, Aircraft safety, and Airborne hazard detection	36
	16. PRICE CODE A03

17. SECURITY CLASSIFICATION OF REPORT	18. SECURITY CLASSIFICATION OF THIS PAGE	19. SECURITY CLASSIFICATION OF ABSTRACT	20. LIMITATION OF ABSTRACT
Unclassified	Unclassified		

NSN 7540-01-280-5500

Standard Form 298(Rev. 2-89)
Prescribed by ANSI Std. Z39-18
298-102

NASA-Langley, 1991